

Large-scale hydrologic and hydrodynamic modeling of the Amazon River basin

Rodrigo Cauduro Dias de Paiva,^{1,2} Diogo Costa Buarque,¹ Walter Collischonn,¹ Marie-Paule Bonnet,² Frédéric Frappart,² Stéphane Calmant,³ and Carlos André Bulhões Mendes¹

Received 24 January 2012; revised 25 October 2012; accepted 18 December 2012; published 4 March 2013.

[1] In this paper, a hydrologic/hydrodynamic modeling of the Amazon River basin is presented using the MGB-IPH model with a validation using remotely sensed observations. Moreover, the sources of model errors by means of the validation and sensitivity tests are investigated, and the physical functioning of the Amazon basin is also explored. The MGB-IPH is a physically based model resolving all land hydrological processes and here using a full 1-D river hydrodynamic module with a simple floodplain storage model. River-floodplain geometry parameters were extracted from the SRTM digital elevation model, and the model was forced using satellite-derived rainfall from TRMM3B42. Model results agree with observed in situ daily river discharges and water levels and with three complementary satellite-based products: (1) water levels derived from ENVISAT altimetry data; (2) a global data set of monthly inundation extent; and (3) monthly terrestrial water storage (TWS) anomalies derived from the Gravity Recovery and Climate Experimental mission. However, the model is sensitive to precipitation forcing and river-floodplain parameters. Most of the errors occur in westerly regions, possibly due to the poor quality of TRMM 3B42 rainfall data set in these mountainous and/or poorly monitored areas. In addition, uncertainty in river-floodplain geometry causes errors in simulated water levels and inundation extent, suggesting the need for improvement of parameter estimation methods. Finally, analyses of Amazon hydrological processes demonstrate that surface waters govern most of the Amazon TWS changes (56%), followed by soil water (27%) and ground water (8%). Moreover, floodplains play a major role in stream flow routing, although backwater effects are also important to delay and attenuate flood waves.

Citation: Paiva, R. C. D., D. C. Buarque, W. Collischonn, M.-P. Bonnet, F. Frappart, S. Calmant, and C. A. B. Mendes (2013), Large-scale hydrologic and hydrodynamic modeling of the Amazon River basin, *Water Resour. Res.*, 49, 1226–1243, doi:10.1002/wrcr.20067.

1. Introduction

[2] The development of large-scale hydrological models has been a subject of important research topics in the past decades. These models, when used in forecast systems, may help to reduce population vulnerability to natural hazards, particularly in the Amazon River basin, where extreme hydrological events have occurred in the past few years, such as the floods of 2009 and 2012 and the droughts in 1996, 2005, and 2010 [Chen *et al.*, 2010; Tomasella *et al.*, 2010; Marengo *et al.*, 2008; Espinoza *et al.*, 2011; Marengo *et al.*, 2011]. Furthermore, complementary to observational

studies [e.g., Frappart *et al.*, 2011a; Azarderakhsh *et al.*, 2011; Alsdorf *et al.*, 2007a], simulation models can support the understanding and quantification of different Amazon hydrological processes such as evapotranspiration, soil and groundwater storages, and river-floodplain hydrodynamics [e.g., Costa and Foley, 1997; Trigg *et al.*, 2009].

[3] Part of recent model developments concerns river and floodplain flow, which is an important factor in the Amazon hydrology. Trigg *et al.* [2009] showed that the Amazon flood wave is subcritical and diffusive. Consequently, backwater effects cause the influence of sea tides on the main river channel to be perceived more than approximately 1000 km upstream the river mouth [Kosuth *et al.*, 2009]. It also causes the influence of the main river over its tributaries [Meade, 1991] and controls droughts [Tomasella *et al.*, 2010]. Floodplain inundation is also an important issue [Bonnet *et al.*, 2008; Alsdorf *et al.*, 2007a, 2010], playing a significant role in large-scale flood propagation [Paiva *et al.*, 2011b; Yamazaki *et al.*, 2011], sediment dynamics [Bourgoin *et al.*, 2007], chemical and ecological conditions [e.g., Junk, 1997; Richey *et al.*, 2002; Melack *et al.*, 2004; Seyler and Boaventura, 2003], and in the climate system due to land surface and atmosphere interactions [Mohamed *et al.*, 2005; Paiva *et al.*, 2011b; Prigent *et al.*, 2011].

¹Instituto de Pesquisas Hidráulicas IPH, Universidade Federal do Rio Grande do Sul UFRGS, Porto Alegre, 91501-970, Brazil.

²Université Toulouse III Paul Sabatier, OMP, Géosciences Environnement Toulouse (UMR 5563 CNRS IRD UPS), Toulouse, France.

³Université Toulouse III Paul Sabatier, OMP, Laboratoire d'Etudes en Géophysique et Océanographie Spatiales (UMR 5566 CNES CNRS IRD UPS), Toulouse, France.

Corresponding author: R. C. D. Paiva, Instituto de Pesquisas Hidráulicas IPH, Universidade Federal do Rio Grande do Sul UFRGS, Porto Alegre, RS 91501-970, Brazil. (rodrigocdpaiva@gmail.com)

[4] Recent modeling developments used different kinds of approaches aiming at sufficiently representing physical processes, but considering computational and input data limitations. River hydrodynamics are generally represented by simplifications of *Saint Venant* equations, including a simplistic relationship between water volume storage and discharge [e.g., *Coe et al.*, 2008], kinematic wave models [*Decharme et al.*, 2011; *Getirana et al.*, 2012] or Muskingum Cunge (MC) type methods [*Collischonn et al.*, 2008; *Beighley et al.*, 2009] and diffusive wave models [*Yamazaki et al.*, 2011] or a full hydrodynamic (HD) model [*Paiva et al.*, 2011a, 2012], where only the last two can represent the aforementioned backwater effects. Although the use of HD models within large-scale distributed hydrological models is still uncommon, they have also been applied in other relatively large-scale problems [*Paz et al.*, 2010; *Biancamaria et al.*, 2009; *Lian et al.*, 2007]. When included, floodplain flows are modeled by different approaches: assuming storage areas having the same river water levels [e.g., *Paiva et al.*, 2011a, 2012; *Yamazaki et al.*, 2011] or considering water exchanges between river and floodplains as a function of river-floodplain water slope [e.g., *Decharme et al.*, 2011]; adopting a composed river floodplain cross sections with 1-D floodplain flow [e.g., *Beighley et al.*, 2009; *Getirana et al.*, 2012]; or considering 2-D floodplain flows [e.g., *Wilson et al.*, 2007; *Trigg et al.*, 2009]. In most of the cases, river bathymetry is approximated by a rectangular shape with parameters estimated as a function of the upstream drainage area (or mean discharge) using empirical relations. Digital elevation models (DEMs) such as the Shuttle Radar Topography Mission (SRTM) DEM [*Farr et al.*, 2007] are used to estimate floodplain bathymetry and river bottom level or surface water slope. Model limitations can be due to the simplifications on representing physical processes and also due to the deficiencies on the aforementioned input data. Consequently, model validations and investigations of the source of errors may guide the improvement of current models.

[5] In this direction, additionally to in situ data commonly used for validation, remote sensing-derived hydrological data sets, such as river stages based on satellite altimetry measurements [*Alsdorf et al.*, 2007b; *Santos da Silva et al.*, 2010], inundation extent [e.g., *Hess et al.*, 2003; *Papa et al.*, 2010], or Terrestrial Water Storage (TWS) derived from the Gravity Recovery and Climate Experimental (GRACE) gravimetry from space mission [*Tapley et al.*, 2004], offer a new opportunity to compare and validate simulation outputs and improve these hydrological modeling approaches.

[6] In this study, we present a hydrologic/hydrodynamic modeling of the Amazon River basin using the MGB-IPH hydrological model [*“Modelo de Grandes Bacias”*; *Collischonn et al.*, 2007] with a full river hydrodynamic module coupled with a simple floodplain storage model [*Paiva et al.*, 2011a] validated against remotely sensed observations. We first present an extensive model validation based on comparisons between model outputs and (1) in situ stream stages and discharges and also water levels derived from ENVISAT RA-2 satellite altimetry data from *Santos da Silva et al.* [2010]; (2) monthly inundation extent from a multisatellite product [*Papa et al.*, 2010]; and (3) GRACE-based TWS from *Frappart et al.* [2010, 2011b]. Then, using the validation results and also sensitivity analyses,

we determine the source of model errors in the Amazon that may be extrapolated to other similar large-scale hydrological models. Finally, the hydrological functioning of the Amazon River basin is explored using the model results, including aspects such as water balance, the surface, soil, and ground water partitioning, and the role of river-floodplain hydraulics on stream flow routing.

2. Methods and Data Sets

2.1. Hydrologic-Hydrodynamic Model

[7] The MGB-IPH model is a large-scale distributed hydrological model that uses physical and conceptual equations to simulate land surface hydrological processes [*Collischonn et al.*, 2007]. It uses a catchment-based discretization and the hydrological response units (HRUs) approach. The simulated vertical hydrological processes include soil water budget using a bucket model, energy budget and evapotranspiration using Penman Monteith approach, interception and soil infiltration, surface runoff based on the variable contributing area concept, and subsurface and groundwater flow generation. The flow generated within the HRUs of each catchment is routed to the stream network using three linear reservoirs, representing the groundwater, subsurface, and surface flow. River flow routing is performed using a combination of either a MC method or a HD model.

[8] The large-scale HD model of MGB-IPH was developed by *Paiva et al.* [2011a] and applied to the Solimões River basin by *Paiva et al.* [2012]. This model differs from the MC model by its capacity to simulate flood inundation and backwater effects. The model solves the full 1-D *Saint Venant* equations [*Cunge et al.*, 1980] for a river network using an implicit finite difference numeric scheme and a Gauss elimination procedure based on a modified skyline storage method. Flood inundation is simulated using a simple storage model [*Cunge et al.*, 1980], assuming that (1) the flow velocity parallel to the river direction is null on the floodplain, (2) the floodplains act only as storage areas, and (3) the floodplain water level equals the water level at the main channel. Consequently, the river-floodplain lateral exchange equals $q_{\text{fl}} = (dz/dt)A_{\text{fl}}(z)/dx$, where x and t are spatial and time dimensions, z is the river water level, and $A_{\text{fl}}(z)$ is the flooded area inside a floodplain unit as described below. Geographic information system (GIS)-based algorithms are used to extract river and floodplain geometry parameters mainly from DEM [*Paiva et al.*, 2011a]. Parameters from a rectangular-shaped river cross section are estimated using geomorphologic equations, and the river bottom level is estimated from the DEM using corrections presented in *Paiva et al.* [2011a]. The algorithm delineates discrete “floodplain units” for each subreach and extracts a z versus A_{fl} curve from the DEM for each of them. Corrections are applied on the DEM as SRTM signal does not penetrate vegetation or surface water and consequently does not provide ground elevation. Flood inundation results in terms of 2-D water levels are computed based on 1-D water level outputs and the DEM.

2.2. Amazon River Basin

[9] The Amazon River basin (Figure 1a) is known as the world’s largest river basin. It has 6 million km² of surface area and drains approximately 15% of the total amount of fresh water dumped into oceans. This region exhibits high

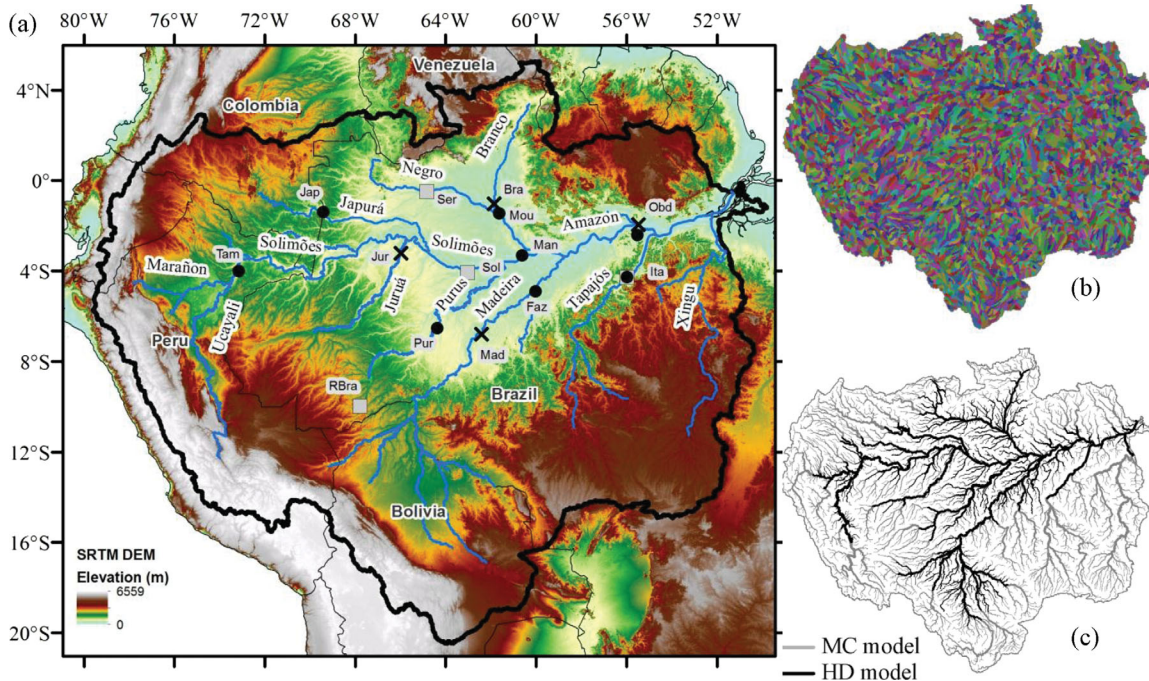


Figure 1. (a) Amazon River basin with its main tributaries, international limits, relief from SRTM DEM, and some of the validation sites. Symbols for the location of the validation sites presented in Figures 3 and 5 are as follows: black circles for the gauge-based discharge series, gray rectangles for the gauge-based water level series, and black crosses for the altimetry-based water level series. Amazon River basin discretization into (b) catchments and (c) river reaches was simulated using the Muskingum Cunge (MC) and hydrodynamic (HD) models.

rainfall rates (average, approximately 2200 mm/yr) with high spatial variability [Espinoza *et al.*, 2009]. Contrasting rainfall regimes are found in the northern and southern parts of the basin, with the rainy season happening in June, July, and August (in December, January, and February) and in the North (South) with more (less) defined wet and dry seasons occurring in the southern and eastern (northern and western) parts of the basin [Espinoza *et al.*, 2009]. The Amazon basin is composed by three morphological units: the Andes with high altitudes and slopes, the Guyanese and Brazilian shields with moderate slopes, and the Amazon plain with very low slopes. Extensive seasonally flooded areas are found at the Amazon plains [Hess *et al.*, 2003; Papa *et al.*, 2010]. In addition, this region is characterized by complex river hydraulics, where the low river slopes cause backwater effects to control part of the river dynamics [Meade, 1991; Paiva *et al.*, 2012]. The above-mentioned characteristics put together give rise to an interesting discharge regime. Rivers draining southern areas have a maximum flow occurring from March to May and a minimum one from August to October. In some other rivers, a weaker seasonal regime can be found, in some cases due to rainfall characteristics and in others, such as the Solimões/Amazon main stem, due to the contribution of lagged hydrographs from northern and southern areas. In the latter, high (low) water occurs generally from May to July (September to November).

2.3. Model Discretization, Parameter Estimation, and Forcing Data

[10] The model discretization into river reaches, catchments, hydrodynamic computational cross sections, and pa-

rameter estimation was carried out using the SRTM DEM [Farr *et al.*, 2007] with 15" resolution (approximately 500 m; see Figure 1a) and GIS-based algorithms described in Paiva *et al.* [2011a]. The Amazon basin was discretized into 5763 catchments, ranging from 100 to 5000 km² (Figure 1b).

[11] An HRU map with 12 classes was developed using the Brazilian and South American soil and vegetation maps [RADAMBRASIL, 1982; Dijkshoorn *et al.*, 2005; Eva *et al.*, 2002] and the Height Above the Nearest Drainage terrain descriptor [Rennó *et al.*, 2008] to identify areas close to rivers where plant-groundwater interactions might take place.

[12] To avoid excessive computing time, we used a combination of the MC and HD models (Figure 1c). River reaches that were simulated with the HD model were selected using the following criteria: (1) river slope lower than 20 cm/km, based on Ponce's [1989] criteria for kinematic wave models and (2) the presence of large floodplains using DEM visual inspection. As a result, approximately 30% of the reaches were simulated using the HD model (Figure 1c). River reaches were then discretized considering the distance between two computational cross sections $\Delta x=10$ km, based on the criteria of the HD model numerical scheme performance [Castellarin *et al.*, 2009; Cunge *et al.*, 1980; Paiva *et al.*, 2011a]. Temporal discretization for both HD and MC models were $\Delta t=3600$ s, based on Courant criteria [Cunge *et al.*, 1980].

[13] River geometry parameters, i.e., river width B (m) and maximum water depth H (m), were estimated as a

Table 1. Geomorphologic Equations Developed to Estimate River Geometric Parameters in Computational Cross Sections^a

River Subbasin	River Width (m)	Maximum Water Depth (m)	
Tapajós and Xingu	$B=0.35 \cdot A_d^{0.62}$	$H=1.91 \cdot A_d^{0.15}$	
Purus and Juruá	$B=3.75 \cdot A_d^{0.36}$	$H=2.35 \cdot A_d^{0.16}$	
Madeira	$B=1.30 \cdot A_d^{0.46}$	$H=1.25 \cdot A_d^{0.20}$	
Negro and Japurá	$B=0.41 \cdot A_d^{0.63}$	$H=1.26 \cdot A_d^{0.20}$	
Solimões	$B=0.80 \cdot A_d^{0.53}$	$H=1.43 \cdot A_d^{0.19}$	
Solimões/Amazon main stream	$B=1.20 \cdot A_d^{0.54}$	$H=22$	$A_d < 400,000 \text{ km}^2$
		$H=20.86+2.86E-6 \cdot A_d$	$A_d < 2,150,000 \text{ km}^2$
		$H=-1.04+1.30E-5 \cdot A_d$	$A_d > 2,150,000 \text{ km}^2$

^aRiver width, B (m); maximum water depth, H (m); upstream drainage area, A_d (km^2).

function of the drainage area A_d (km^2), using geomorphologic equations developed from river cross sections surveys achieved at stream gauge locations provided by the Brazilian Water Resources Agency (Agência Nacional das Águas (ANA)). We developed different sets of geomorphologic equations for six sub-basins within the Amazon defined by its major tributaries, as shown in Table 1 (see also Figure 1a).

[14] River bottom levels were estimated from the DEM using Paiva *et al.* [2011a] algorithms and $H_{\text{veg}}=17$ m (vegetation height) to eliminate DEM errors due to vegetation. In addition, when using DEM to extract water level versus flooded area curves, all of its pixel values (Z_{DEM}^*) were corrected using $Z_{\text{DEM}}^* = Z_{\text{DEM}} - H_{\text{veg}}$, except for areas with low vegetation, according to the HRU map.

[15] Meteorological data were obtained from the CRU CL 2.0 data set [New *et al.*, 2002], which provides monthly climatological values calculated using interpolated data from ground stations for the period between 1960 and 1990 at a spatial resolution of $10'$, which is in accordance with the low density of meteorological stations in the Amazon. We also used TRMM daily precipitation data provided by algorithm 3B42 [Huffman *et al.*, 2007], with a spatial resolution of $0.25^\circ \times 0.25^\circ$ for the 12-year period 1998–2009.

[16] The MGB-IPH model parameters related to soil water budget were calibrated against discharge data from stream gauges using the MOCOM-UA optimization algorithm [Yapo *et al.*, 1998; Collischonn *et al.*, 2007] for the 1998 to 2005 time period, using the model performance statistics E_{NS} , E_{NSlog} , and ΔV , as described in the next section. For parameter calibration, model runs were used only within the MC model to avoid high computational costs, and therefore, we used only stream gauges located in river reaches simulated with the MC model (Figure 1c). Gauges located in reaches simulated with the HD model were used only for validation. The calibration procedure optimized six parameters related to soil water budget for each HRU (the maximum water storage in the upper layer of soil W_m ; three equivalent hydraulic conductivities K_{bas} , K_{int} , and K_{cap} ; the parameter from the variable contributing area model for runoff generation b), and three parameters related to surface, subsurface, and base flow residence time (C_s , C_i , and T_{KB}) following Collischonn *et al.* [2007]. We optimized these parameters for each large river sub-basin, giving rise to tens of different parameter sets with the following median values and ranges (5% and 95% percentiles): $W_m=282$ (30–1800) mm, $b=0.48$ (0.02–4.6), $K_{\text{bas}}=1.2$ (0.03–6.9) mm/day, $K_{\text{int}}=5.2$ (0.2–200) mm/day, $K_{\text{cap}}=0.02$ (0–0.26) mm/day, $C_s=12.4$ (5.6–35.5), $C_i=10.0$

(3.9–1379), $T_{\text{KB}}=99$ (18–386) days. In some cases (10%), calibrated parameters were out of these ranges, possibly due to input data errors (e.g., precipitation as discussed later) or even limitations in the model. Vegetation parameters used in energy balance and evapotranspiration computations (e.g., leaf area index, superficial resistance, albedo, and vegetation height) were taken from Shuttleworth [1993]. The only parameter related to the HD model is the Manning's coefficient and it was not calibrated using the MOCOM-UA algorithm. Instead, we used different values for different large river basins aiming at fitting hydrographs in the largest Amazonian rivers (0.035 in almost all the Amazon basin, 0.025 in the lower Madeira basin, 0.030 in the upper Madeira, upper Solimões, and upper Negro basins, and 0.040 in upper part of Brazilian Solimões River).

2.4. Model Validation Approach

2.4.1. Discharge

[17] Daily discharge results were compared with data from 111 stream gauges (Figure 2) provided by the Brazilian Agency for Water Resources (ANA), the Peruvian and Bolivian National Meteorology and Hydrology Services (Servicio Nacional de Meteorología e Hidrología), and the Hydrology, Biogeochemistry and Geodynamic of the Amazon Basin (HYBAM) program (<http://www.ore-hybam.org>) for the 1999–2009 period. Values from the HYBAM database provided better discharge estimates in the central Amazon as it is based on both stages and water slope and, consequently, is able to represent looped rating curves.

2.4.2. Water Level

[18] Simulated daily water levels were validated against stream gauge records and radar altimetry data. We used 69 stream gauges for the 1998 to 2005 period selected from ANA's database (see Figure 5).

[19] We also compared the computed water levels with ENVISAT satellite altimetry data. ENVISAT satellite has a 35-day repeat orbit and an 80 km intertrack distance. The database used is an extension of the one presented in Santos da Silva *et al.* [2010]. It consists of 212 altimetry stations (deduced from the intersection of a satellite track with a water body) with water level time series reported to EGM08 geoid for the 2002 to 2009 period. Altimetry stations are located mainly along the Solimões, Amazon, Juruá, Japurá, Madeira, Negro, and Branco Rivers (see Figure 5). ENVISAT data selection techniques preconized by Santos da Silva *et al.* [2010] result in approximately 10–40 cm water level accuracy. As water level model results are

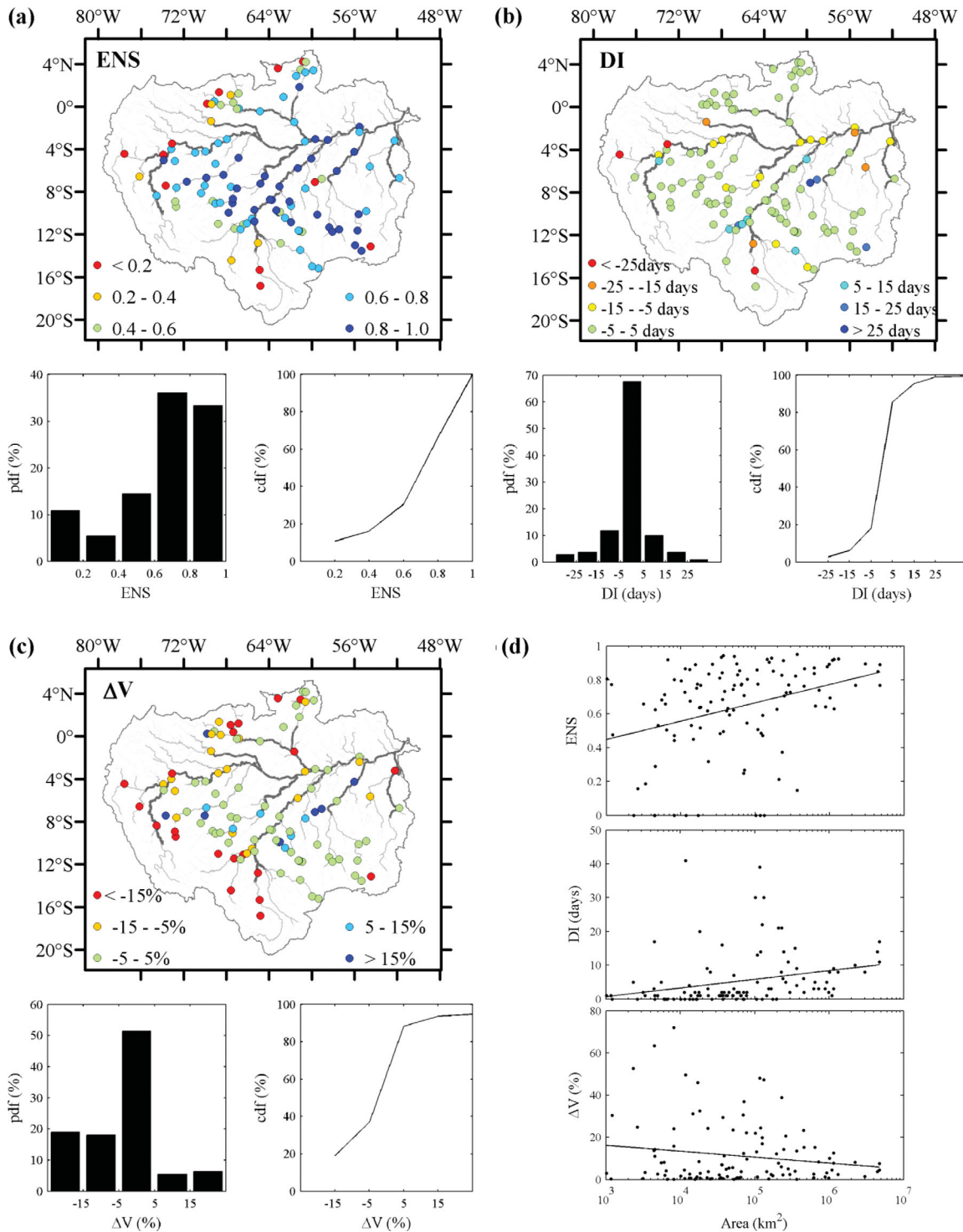


Figure 2. Validation of daily discharge derived from MGB-IPH model against stream gauge observations. Spatial distribution and probability (pdf) and cumulative (cdf) distribution functions of model performance statistics: (a) Nash and Sutcliffe index (E_{NS}), (b) delay index (DI), (c) volume error (ΔV), and (d) relationship between upstream drainage area and model performance statistics.

based on the SRTM DEM, it became necessary to convert ENVISAT water levels from their initial EGM08 geoidal reference to an EGM96 geoidal reference. We used the programs provided by the National Geospatial-Intelligence Agency (<http://earth-info.nga.mil/>) to perform the conversion.

2.4.3. Flood Extent

[20] Flood inundation results were compared with a multisatellite monthly global inundation extent data set at an approximately 25 km × 25 km spatial resolution and available over the 1993–2004 period [Papa *et al.*, 2010]. This product was derived from multiple-satellite observations,

including passive (Special Sensor Microwave Imager) and active (ERS scatterometer) microwaves along with visible and near-infrared imagery (advanced very high-resolution radiometer). This data set was already used for validating other large-scale streamflow routing and flood models [e.g., Decharme et al., 2011; Yamazaki et al., 2011]. It is provided on an equal area grid of $0.25^\circ \times 0.25^\circ$ at the Equator where each pixel has 773 km^2 of surface area. Considering this, for model validation, we computed daily water depth grids at a $15''$ resolution ($\sim 500 \text{ m}$) based on simulated water levels and the DEM, as described in Paiva et al. [2011a], and then we resampled it into an approximately $25 \text{ km} \times 25 \text{ km}$ grid to compute monthly inundation extent only for the 1999–2004 time period.

2.4.4. Terrestrial Water Storage

[21] The GRACE mission, launched in March 2002, provides measurements of the spatiotemporal changes in Earth's gravity field. Several recent studies have shown that GRACE data over the continents can be used to derive the monthly changes of the TWS [Ramillien et al., 2005, 2008; Schmidt et al., 2008] with an accuracy of approximately 1.5 cm of equivalent water thickness when averaged over surfaces of thousands of square kilometers. These TWS changes estimates over land include all hydrological compartments, such as rivers, floodplains, lakes, soil, and groundwater. We used the level 2 land water solutions (RL04) produced by GFZ, JPL, and CSR with a spatial resolution of approximately 333 km and an accuracy of $15\text{--}20 \text{ mm}$ of water thickness. These are smoothed solutions using a 400 and 500 km half-width Gaussian filter and provided at $1^\circ \times 1^\circ$ and at a monthly time interval. They are also postprocessed using an independent component analysis approach [Frappart et al., 2010], which demonstrates a strong capacity for removing the north-south stripes polluting the GRACE solutions [Frappart et al., 2011b].

[22] To derive TWS estimates from the MGB-IPH model, we used the following procedure. For each catchment, total water storage S (considering river, floodplain, surface, soil, and ground waters) is related to precipitation (P), evapotranspiration (ET), river inflow (I), and outflow (O) by the continuity equation $dS/dt = (P - ET) \cdot A_d + I - O$, where A_d is the catchment drainage area and t is time. For each day, water storage was derived as $S_{t+1} = S_t + [(P_{t,t+1} - ET_{t,t+1}) \cdot A_d + I_{t,t+1} - O_{t,t+1}] \Delta t$, where Δt is the time interval, similarly as used by Getirana et al. [2011] at the basin scale for the Negro River basin.

[23] Then, to derive model TWS estimates comparable with GRACE data, we smoothed MGB-IPH TWS values using a 450 km half-width Gaussian filter. Moreover, as the original GRACE spatial resolution is larger than $1^\circ \times 1^\circ$, we chose to resample both GRACE and MGB-IPH data to a $4^\circ \times 4^\circ$ grid (Figure 9). For each $4^\circ \times 4^\circ$ pixel, TWS derived from GRACE was computed as a simple average of the $1^\circ \times 1^\circ$ pixels, and TWS from MGB-IPH model was estimated as the weighted mean of TWS of all catchments inside each $4^\circ \times 4^\circ$ pixel, using catchment drainage area as weight. Finally, we computed TWS anomalies using the 2003–2009 long-term average.

2.4.5. Model Performance Statistics

[24] MGB-IPH model results were compared with the observations using some statistics commonly used in hydrological modeling studies: (1) Nash-Sutcliffe coeffi-

cient E_{NS} ; (2) log-Nash-Sutcliffe coefficient E_{NSlog} [Colli-schonn et al., 2007], i.e., E_{NS} computed using a logarithm transformation on discharge time series to focus on low flows; (3) relative bias ΔV (%) or BIAS; and (4) Pearson's correlation coefficient R . A “delay index” (DI, in days) [Paiva et al., 2011b] was used to measure errors related to the time delay between simulated and observed hydrographs. It is computed using the cross correlation function $R_{xy}(m)$ from simulated (x) and observed (y) time series, where DI equals the value of the time lag m and where $R_{xy}(m)$ is at maximum. Positive (negative) DI values indicate delayed (advanced) simulated hydrographs. Furthermore, we measured the water level, the TWS, and the flood extent amplitude error $A' = 100(A_{calc} - A_{obs})/A_{obs}$, where A_{calc} and A_{obs} are the simulated and observed amplitudes. The amplitude A of a given variable is defined here as the difference between its 95% and 5% percentiles. Due to differences in water levels datum reference and as GRACE actually measures TWS changes, for these variables, all model performance statistics (except BIAS) were computed after removing the long-term average.

3. Model Validation

3.1. Discharge

[25] Validation against river discharges shows a good performance of the MGB-IPH model. According to Figure 2, in 70% of the stream gauges, the $E_{NS} > 0.6$ and model represents mean discharge with accuracy, as volume errors $|\Delta V| < 15\%$ in 75% of the gauges. According to E_{NS} and ΔV values (Figure 2d), the model performs better in large rivers, although it is sufficiently good in the smaller ones ($E_{NS} > \sim 0.5$ and $|\Delta V| < \sim 20\%$). The flood waves' timing is also well represented by the model and $DI < 5$ days in 70% of the stream gauges. DI values increase in large rivers and, for example, simulated flood wave is 5–15 days in advance in the Solimões/Amazon main stem. However, these values can be considered small if compared with the large flood traveling times of Amazon large rivers (a couple of months).

[26] Most of the errors are concentrated in rivers draining westerly areas in Bolivia, Peru, and Colombia, where the model underestimates discharges. However, these errors can compensate each other and provide feasible discharge results in downstream rivers. We speculate that such errors are a consequence of the poor quality of TRMM 3B42 rainfall data set in these areas, which are poorly monitored and/or mountainous. This is supported by the sensitivity analysis presented in section 4, which shows that errors in precipitation cause large changes in mean discharge as well as in water depths and flood extent. Errors in satellite rainfall estimates over the Andean region of the Amazon were also shown by Condom et al. [2010] and by Tian and Peters-Lidard [2010] in a global map of uncertainties of satellite precipitation estimates.

[27] Results for the main Amazon tributaries are promising (Figure 3). A very good model performance can be found in Juruá and Purus River basins, where the model is able to represent complex (noisy) hydrographs in the upper part and flood waves attenuations as they travel downstream (see Figure 3c for lower Purus). For the Madeira River basin, errors are found mostly in the Bolivian region

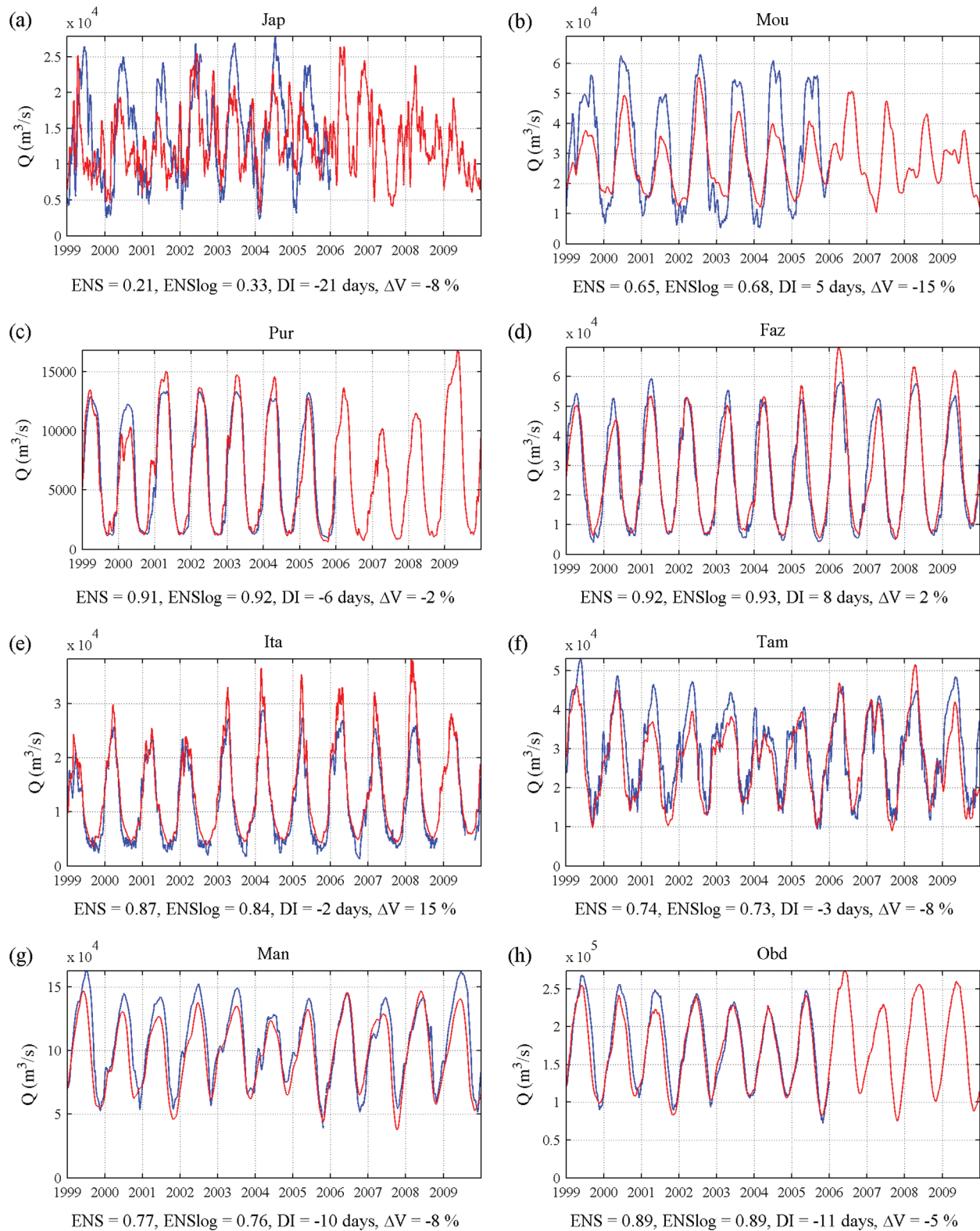


Figure 3. Observed (blue line) and simulated (red line) daily discharge in (a) Japurá River (Jap), (b) lower Negro River at Moura (Mou), (c) lower Purus River (Pur), (d) lower Madeira River at Fazenda Vista Alegre (Faz), (e) lower Tapajós River at Itaituba (Ita), (f) Solimões River at Tamshiyacu (Tam), (g) Solimões River close to confluence with Negro at Manacapuru (Man), and (h) Amazon River at Obidos (Obd). Sites are indicated in Figure 1.

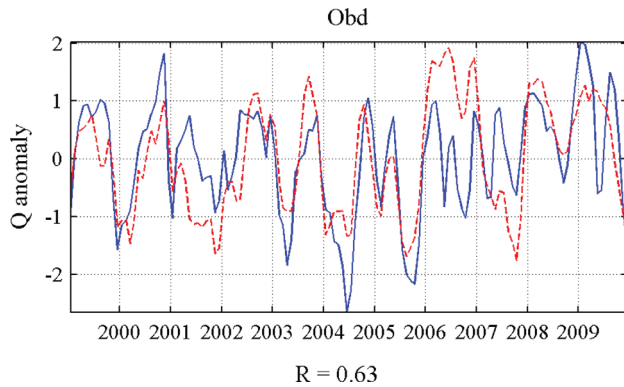


Figure 4. Observed (blue line) and simulated (red line) anomalies of monthly discharges in the Amazon River at Obidos (Obd).

(Figure 2); however, in most of the Brazilian tributaries and in the Madeira main stem, the discharge is well represented (Figure 3d). Satisfactory model results are also found at Tapajós River basin (Figure 3e), where hydrographs are mostly dominated by direct runoff and base flow, as large floodplains are not present (see Figure 7). At Japurá River, which drains parts of the Andes of Colombia and Peru, the model results are poor, as shown in Figure 3a. At Negro River basin, better results are found mostly in the

Branco River basin (northeast) and worst results in the upper Negro River (northwest); however, it shows improvement in lower Negro River.

[28] Although there are large errors in the upper part of the Solimões river basin in Peru, flood waves are well represented in the Solimões/Amazon main stem, as shown in Figures 3f and 3g at Tamshiyacu and Manacapuru, respectively. At Óbidos site, located close to the Amazon River outlet, results (Figure 3h) show a good performance of the MGB-IPH model. E_{NS} is high (0.89), the volume error is low (-4.6%), and the flood wave is advanced in only -11 days. Hydrological extremes such as the 2005 drought and the 2009 flood are well represented (Figure 3h), and the model captured interannual variability (Figure 4).

3.2. Water Levels

[29] Validation against water levels from stream gauges shows that the model is performing well in the major tributaries of the Amazon (Figure 5). $E_{NS} > 0.60$ in 55% of the stream gauges and $R > 0.8$ in 80% of the cases. Water level results are similar to the observations in large rivers, such as in the Solimões River (Figure 6a), and also in smaller rivers where fast flood waves are present, such as in the Acre River in the upper Purus basin (Figure 6b). Timing of flood waves are well represented in most gauges (DI < 5 days in 80% of the cases). Validation against ENVISAT satellite altimetry data also shows that the model performs

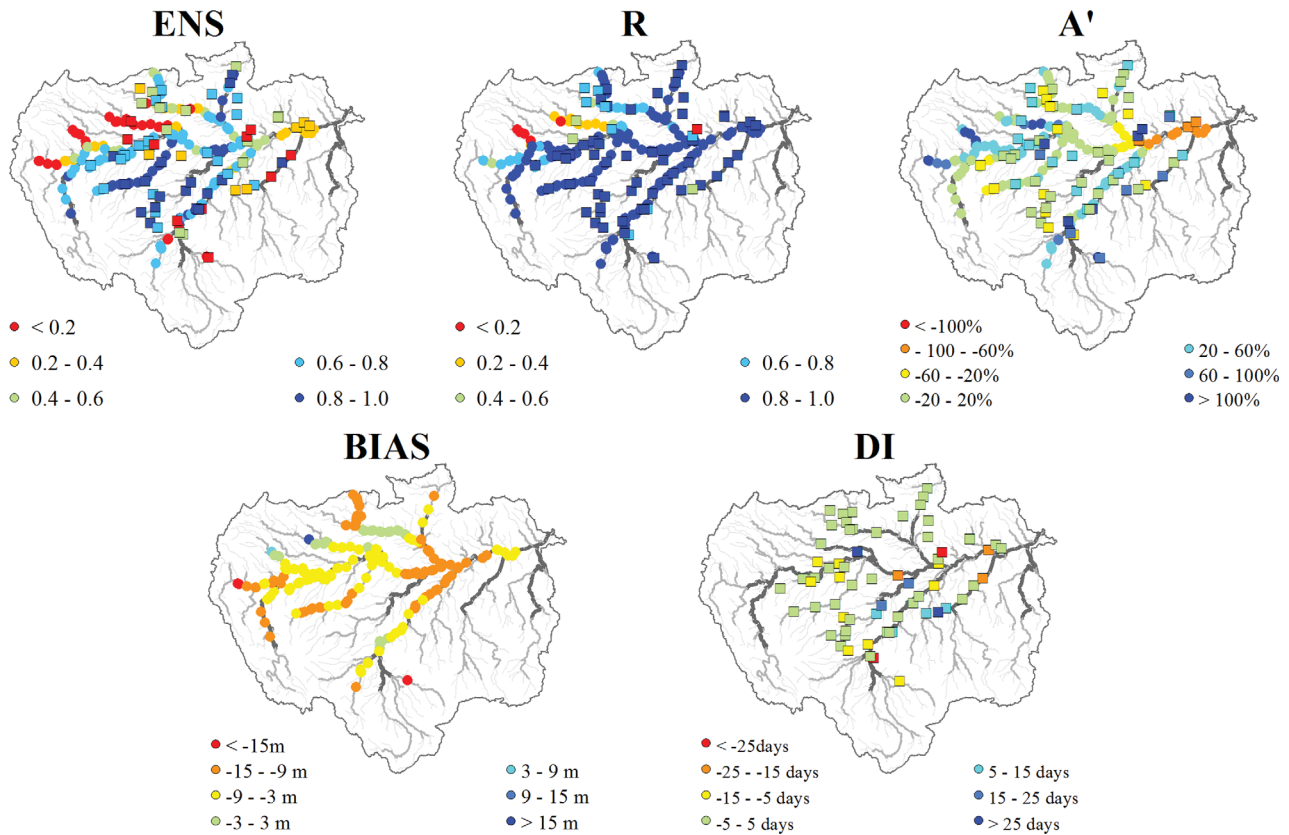


Figure 5. Validation of daily water levels derived from MGB-IPH model against stream gauge observations (squares) and ENVISAT satellite altimetry data (circles). Spatial distribution of model performance statistics: Nash and Sutcliffe index (E_{NS}), Pearson’s correlation coefficient (R), amplitude error (A'), delay index (DI), and bias (BIAS).

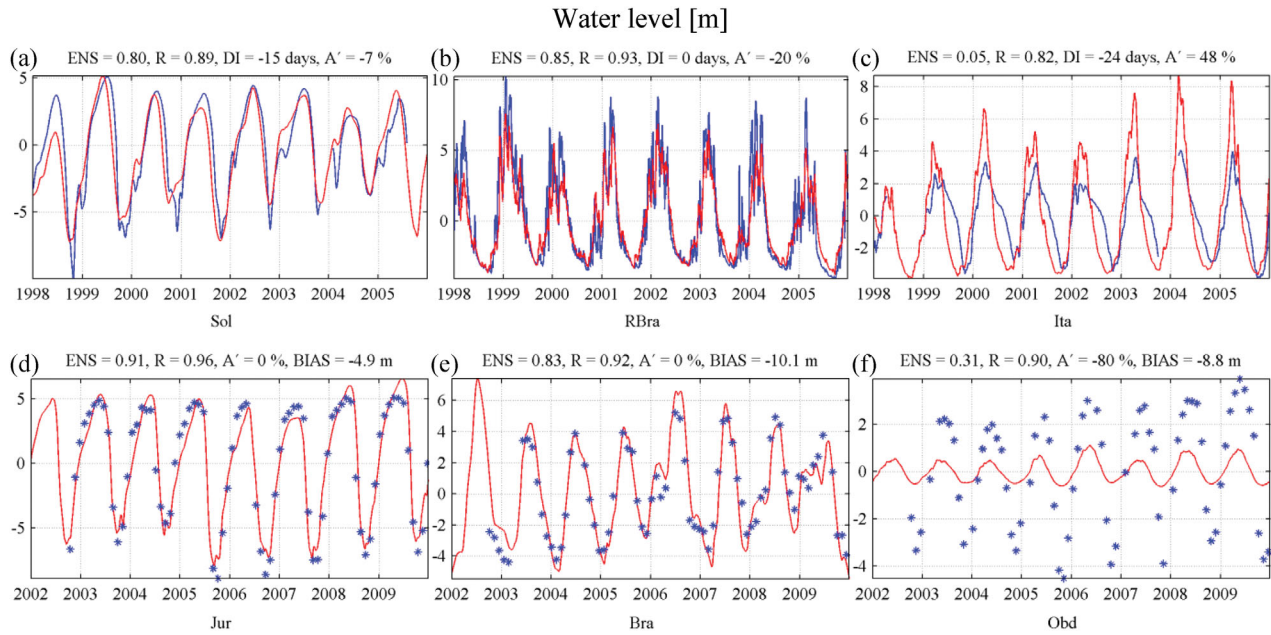


Figure 6. Simulated (red line) and observed daily water levels from stream gauges (blue line) and derived from ENVISAT satellite altimetry data (blue points) at (a) Solimões River (Sol), (b) upper Purus River basin at Acre River in Rio Branco (RBra), (c) lower Tapajós River at Itaituba (Ita), (d) lower Juruá River (Jur), (e) lower Branco River (Bra), and (f) Amazon River at Óbidos (Obd). Sites are indicated in Figure 1.

well, mostly in central Amazon, Solimões, Juruá (Figure 6d), Branco (Figure 6e), and Madeira River, and $E_{NS} > 0.6$ in 60% of the virtual stations.

[30] However, large errors are found in some sites. A part of them is located in rivers draining poorly monitored and/or mountainous areas where discharges are also poorly simulated (see section 3.1). In some of the stream gauges, despite the fact that the observed and simulated water levels are highly correlated and DI values are low, large amplitude errors are present, which indicates that model errors are due to the uncertainty of local cross section geometry, e.g., river width. In other sites located mainly close to a confluence with a large river (e.g., lower Tapajós River in Figure 6c), there are large errors of timing and shape of flood waves, probably because either simulated or observed water levels are controlled by both upstream flow and backwater effects. In this case, errors in river bottom level estimates could give rise to errors in the extension of backwater effects and in the timing of flood waves [similar to Paiva *et al.*, 2012]. We also found a large bias between model and ENVISAT water levels, ranging from -3 to -15 m (Figure 5). Smaller bias values were found by Yamazaki *et al.* [2012b] in the Amazon main stem, and differences may be associated to different methods for extracting errors from the DEM. In addition, important errors are found in lower Amazon River (Figures 5 and 6f). The correlation with the observations is very high; however, the model strongly underestimates the amplitude of water levels. Such errors could be due to errors in river width estimates and also in the DEM data and therefore floodplain geometry errors. These problems cause errors in flood extent and consequently in river-floodplain volume exchanges, as supported by the sensitivity analysis presented in section 4.

3.3. Flood Extent

[31] The overall inundation extent results from the MGB-IPH model are similar to remote sensing estimates from Papa *et al.* [2010], showing the seasonal variation of flood extent and the north-south contrast, with flood peaks occurring in DJF and MAM at the Bolivian Amazon, in MAM and JJA at central Amazon, and JJA in the north (Figure 7).

[32] The model provides total inundation extent similar to remote sensing estimates (Figure 8) for the whole Amazon basin, with relatively good model performance statistics: $E_{NS}=0.71$, $R=0.92$, $A'=-26\%$, and $BIAS=-7\%$. However, analyses in different regions (rectangles in Figure 7) show that errors are compensated when generating the overall estimate.

[33] The best model results are found in central Amazon (Figure 8), where a relatively low amplitude error (12%), bias (14%), and high correlation coefficient (0.85) are found. In the Peruvian Amazon (Figure 8c), the model overestimates flood extent although the seasonal variation is well represented, whereas in the Bolivian Amazon (Figure 8b), low water period and seasonal variation are well captured by the model; however, flood at high water period is underestimated (DJF and MAM). In lower Amazon (Figure 8d), bias is only -30% and the seasonal variation is well represented ($R=0.90$). However, the model underestimates the amplitude and flood at the high water period, leading to a low E_{NS} value. This is in accordance with errors in water levels presented in section 3.2.

[34] It is noteworthy that a part of the errors could come from the remote sensing observations. A previous and similar data set [Prigent *et al.*, 2007] seems to overestimate flood extent in the lower Amazon and underestimate it in

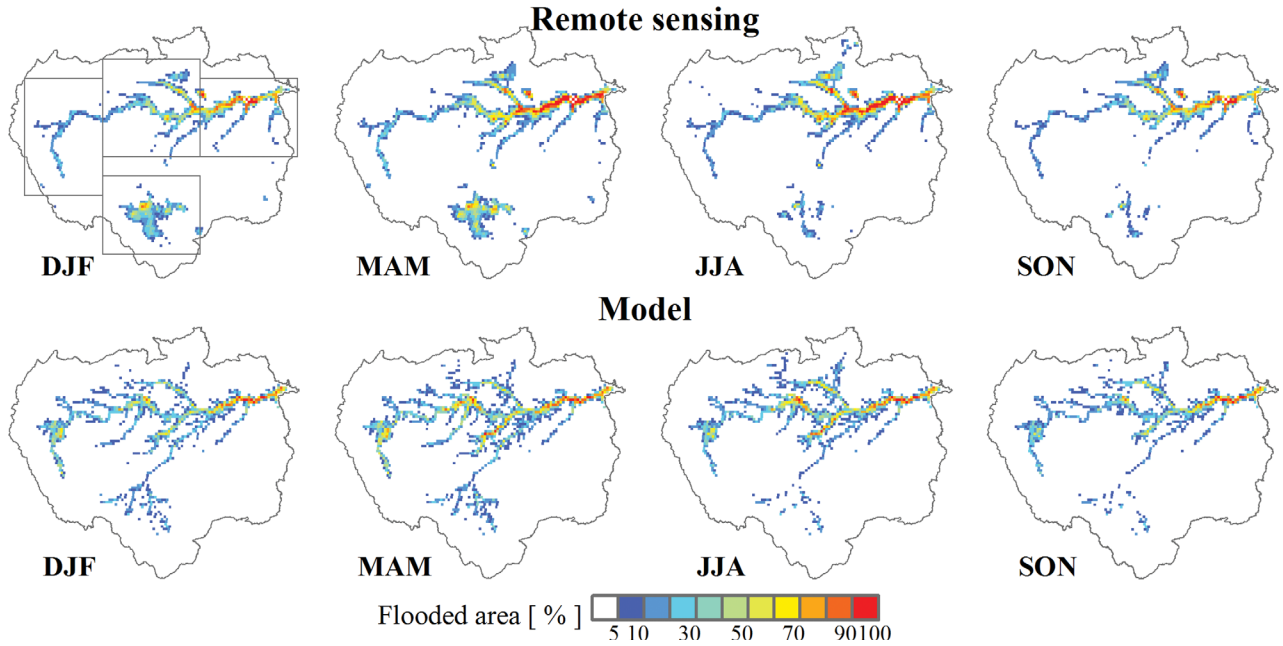


Figure 7. Seasonal variation of inundation extent derived from MGB-IPH model and remote-sensing estimates from *Papa et al.* [2010]. Average values for DJF, MAM, JJA, and SON seasons were computed for the 1999–2004 period.

the Solimões floodplain (central Amazon) if compared with *Hess et al.* [2003] dual season estimates for 1996 high water and 1995 low water periods.

[35] Errors in flood extent may be due to uncertainty in river-floodplain geometry parameters, as presented in section 4. For example, important errors are found in water levels and inundation extent in the lower Amazon River. In

both cases, model results are highly correlated with the observations; however, the model underestimated the amplitude of water levels and flooded area. We speculate that the errors in lower Amazon River are due to river width errors and DEM errors. We used a coarser version of SRTM DEM with an approximately 500 m resolution instead of 90 m, whereas floodplain flows can be partly

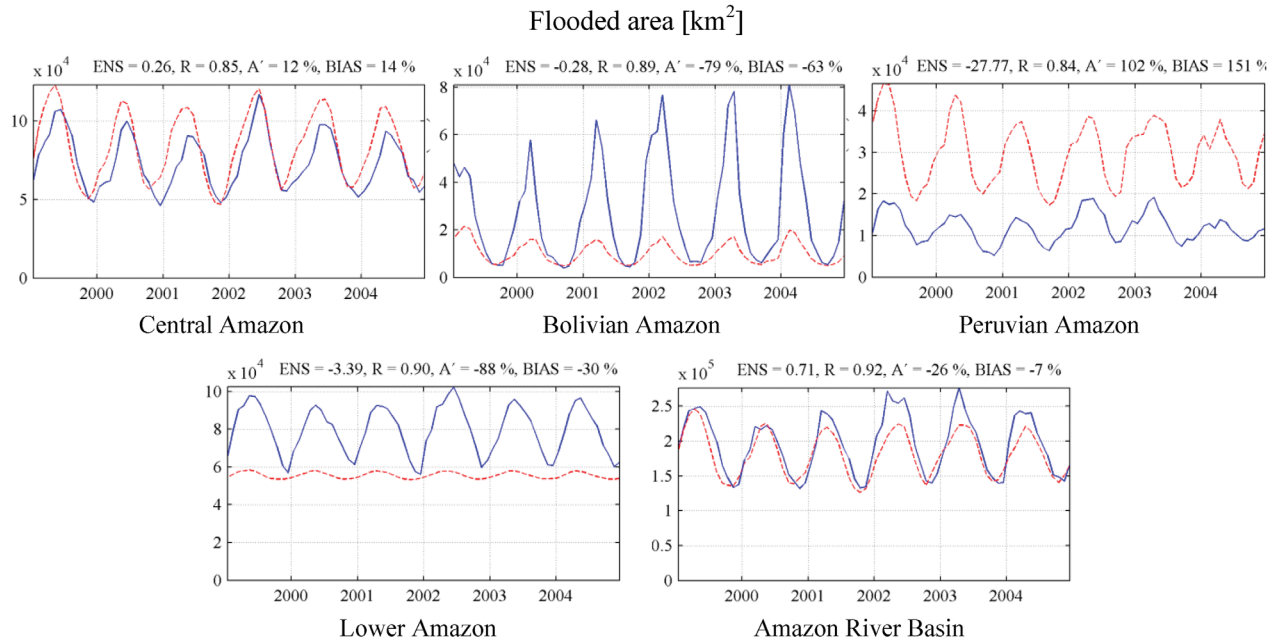


Figure 8. Monthly flooded area derived from MGB-IPH model (red dashed line) and remote-sensing estimates from *Papa et al.* [2010] (blue line) at central Amazon (8°S 70°W to 2°N 60°W), Bolivian Amazon (18°S 70°W to 10°S 60°W), Peruvian Amazon (12°S 78°W to 0°S 70°W), lower Amazon (8°S 60°W to 0°S 50°W), and Amazon River basin. Regions are presented in Figure 7.

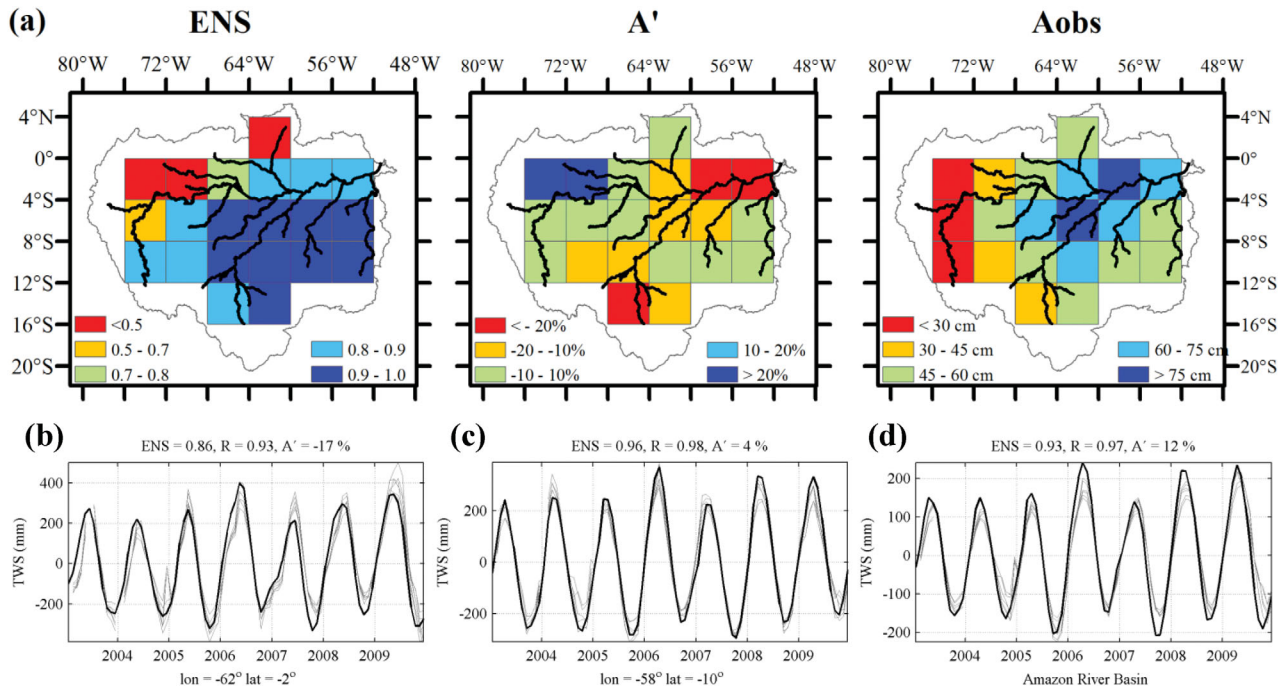


Figure 9. Validation of monthly terrestrial water storage (TWS) derived from MGB-IPH model against GRACE estimates (2003–2009). (a) Spatial distribution of Nash and Sutcliffe index (E_{NS}), amplitude error (A'), and observed amplitude (A_{obs}). Monthly time series of TWS derived from MGB-IPH model (black) and six GRACE solutions (gray) in (b) lower Negro River Basin ($4^\circ \times 4^\circ$ pixel centered in 62°W , 2°S), (c) Upper Tapajós River Basin (58°W , 10°S), and (d) Amazon River Basin. Statistics are presented for CSR solution with 400 km Gaussian filter.

controlled by smaller scale topography such as small channels [Trigg *et al.*, 2012]. Besides, the SRTM DEM has systematic errors related to vegetation and surface water effects [Sun *et al.*, 2003]. We corrected these errors using methods presented in Paiva *et al.* [2011a] for river bottom level estimation and subtracting a constant value of $H_{veg}=17$ m in all DEM pixels, except where there is low vegetation. However, vegetation height may be variable even in forested areas. For example, in lower Amazon, large marginal lakes are present in floodplain [e.g., Melack and Hess, 2010; Bonnet *et al.*, 2008], and due to the correction applied in DEM, they are always flooded in the model simulation. Furthermore, a small water level variation leads to less river-floodplain volume exchanges.

3.4. Terrestrial Water Storage

[36] Analyses show that the model provides TWS in good accordance with GRACE estimates. E_{NS} values for TWS over the whole Amazon is 0.93, the correlation coefficient is high (0.97), and the amplitude error is low (12%). Figure 9d shows that interannual variability is represented by the model, including the 2005 drought and the 2009 flood.

[37] We also examined results in 21 square subregions with spatial resolution of $4^\circ \times 4^\circ$. $E_{NS}<0.8$ and $R<0.9$ only in five areas, and these are found mostly in the north-west part of the Amazon and in the upper Branco River basin, possibly due to the same errors reported in discharge results related to the precipitation forcing. In addition, these

areas are concentrated in the border of the river basin, where the Gaussian filter applied to the model results may have added errors. In other parts of the Amazon, results were provided in accordance with GRACE estimates (e.g., Figures 9b and 9c). Amplitude errors are larger than 20% only in five subregions, located in west and in lower Amazon River. In the latter, errors are in accordance with the underestimation of water level and flood extent amplitude presented in sections 3.2 and 3.3.

4. Sensitivity Analysis

[38] We performed a sensitivity analysis to investigate the sources of model errors and also the physical functioning of the Amazon River basin. The model sensitivity to six model parameters/variables was evaluated: river width, Manning's roughness coefficient, river bottom level, precipitation, flooded area, and maximum soil storage. In all cases, each parameter/variable was equally perturbed in all Amazon river basin by the factors +50, +20, 0, -20, and -50%, except for river bottom level where we used +3, +1, 0, -1, and -3 m. Results were evaluated in terms of discharge close to the basin outlet at Óbidos station (Obd site at Figure 1), water depth at central Amazon at Manacapuru station (Man site at Figure 1), and total flooded area (Figures 10 and 11) using climatological values computed from the 1999 to 2009 time period.

[39] An important interaction between water levels, flooded areas, and discharge occurs during flood waves

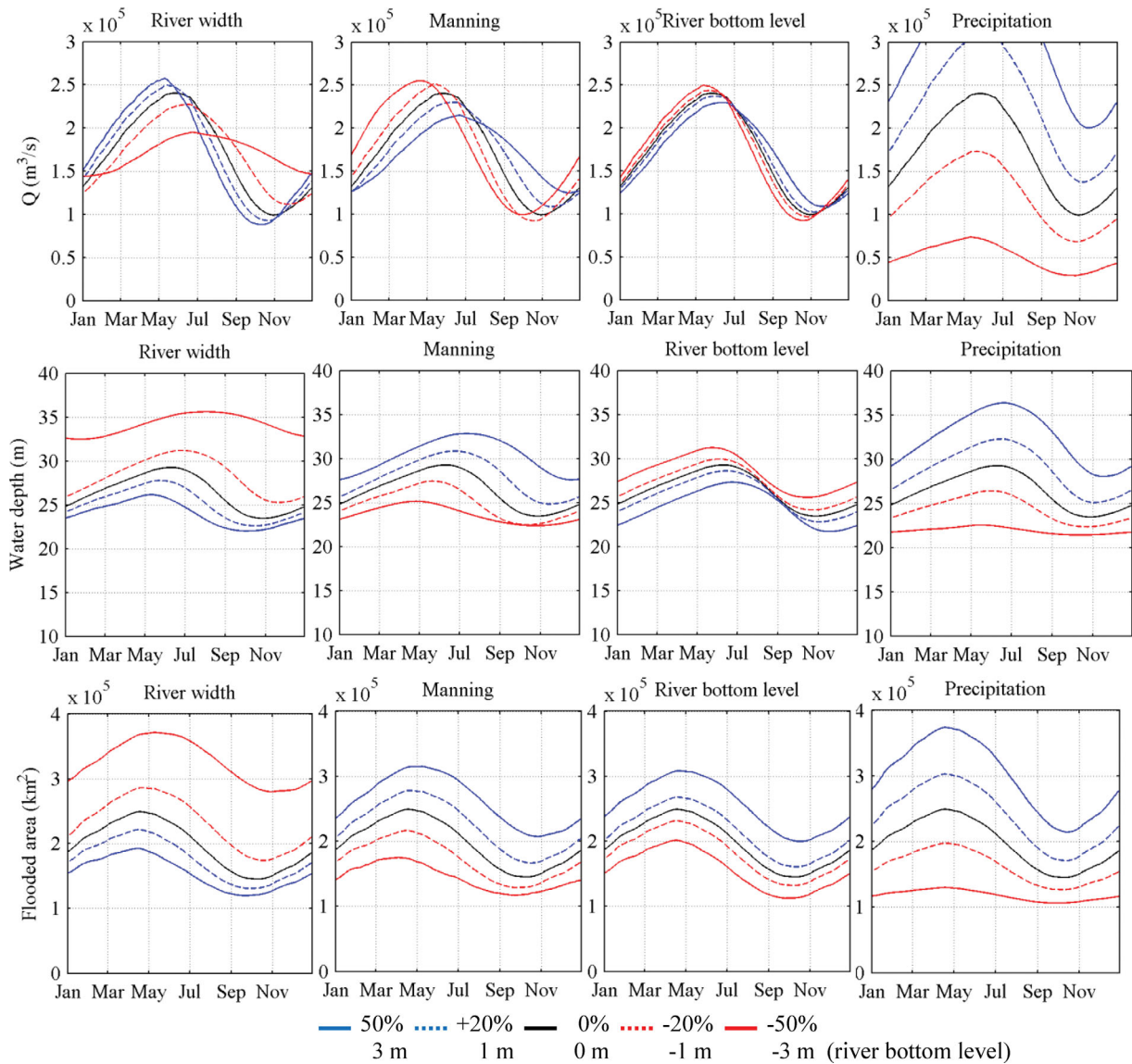


Figure 10. Sensitivity analysis: climatology of discharge at Óbidos (Obd), water depth at Manacapuru (Man), and total flooded area derived from simulations using perturbed values of river width, Manning’s coefficient, river bottom level, and precipitation.

traveling (Figure 10). A decrease in river width causes a large increase in water depths and levels, consequently an increase of flooded areas occurs and flood waves are attenuated and delayed in a couple of months, causing minor flood flows and droughts, although the mean discharge does not change. Still, an increase in river width decreases water depth and flood inundation, resulting in advanced flood waves and major high water discharges. An explanation would be that larger amounts of water are stored and released across the floodplains, causing larger flow travel times. An inverse effect is observed perturbing Manning’s roughness coefficient. River width and Manning’s coefficient results are similar to those discussed by Yamazaki *et al.* [2011] about river and floodplain interactions and flood wave travel times.

[40] Increasing river bottom levels causes, at first, a smaller difference between river and floodplain bottom lev-

els, and as a result, flooding is easier to occur. Consequently, flood extension increases and the aforementioned effect takes place with a delayed flood wave. However, now water depth decreases possibly because larger amounts of water enter in floodplains.

[41] Precipitation is the most sensitive variable (Figure 10) and increasing it dramatically increases mean discharge, water depths, and flood extent. In addition, the same river-floodplain interaction takes place and flood waves are delayed and attenuated, although changes in mean values are much more pronounced.

[42] Positive changes in flooded areas (from the z versus A_{fl} curve derived from the SRTM DEM) cause a similar effect than that observed in the river bottom level, with a decrease in water depths and delayed and attenuated flood waves (Figure 11). Finally, we examined maximum soil water storage (Figure 11), the most sensitive parameter of

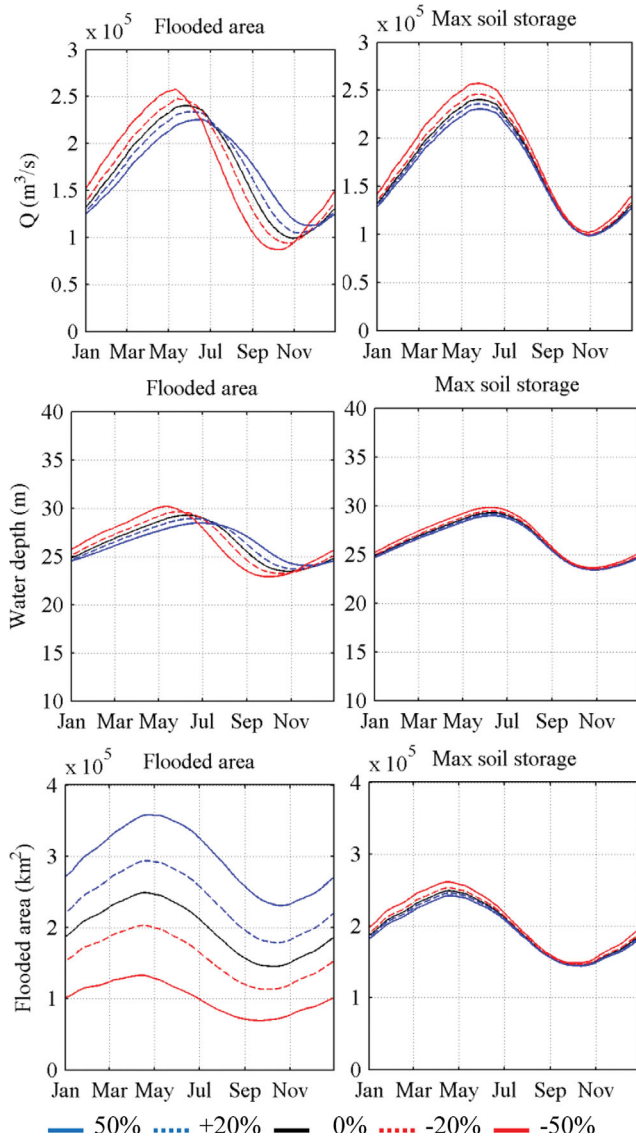


Figure 11. Sensitivity analysis: climatology of discharge at Óbidos (Obd), water depth at Manacapuru (Man), and total flooded area derived from simulations using perturbed values of flooded area and maximum soil storage.

vertical water/energy balance of the MGB-IPH model [Colischonn, 2001]. Positive perturbations decrease all variables, probably because larger amounts of available water in the soil facilitate larger evapotranspiration rates. However, the sensibility of this parameter is not as pronounced as the others.

[43] It is worth mentioning that we evaluated errors equally distributed over the entire basin and that local uncertainties can cause different kinds of errors in discharges, water depths, and flood extent. For example, errors in river width in a small reach may cause errors in both the mean and amplitude of water depths and consequently in local flood extent; however, these errors may not have a major influence over other parts of the basin.

[44] The analysis shows that input data uncertainty might play an important role in model errors. The model results are very sensitive to river-floodplain parameters, indicating

the need to improve current estimation methods, which are based mostly in geomorphological relations and information from the SRTM DEM. These conclusions are consistent with recommendations from other modeling studies using global river-flood models [Decharme *et al.*, 2011; Yamazaki *et al.*, 2011] and a flood inundation model [Wilson *et al.*, 2007]. Data from field campaigns could be used; however, methods using remote sensing to estimate river width and bottom level should also be investigated, such as in Durand *et al.* [2010a]. Moreover, either a new DEM or a more sophisticated correction of the SRTM DEM is needed, removing vegetation height in forested areas and estimating bottom level of floodplain lakes. Vegetation effects could be removed, for example, using a global vegetation height map, such as in Simard *et al.* [2011]. Water level effects could be removed using a combination of satellite altimetry water levels and flood extent data, such as the techniques used by Frappart *et al.* [2008, 2011a] to estimate floodplain volumes variation. DEM corrections to allow better flow connectivity in small channels connecting floodplains such as those presented by Yamazaki *et al.* [2012a] could also be used. Additionally, data from the future surface water and ocean topography mission could also be used [Durand *et al.*, 2010b].

5. Aspects of Amazon Hydrological Processes

5.1. Water Balance

[45] Figure 12 presents the main components of water balance of the Amazon basin, comprising mean precipitation (P), evapotranspiration (ET), and discharge (Q) at Óbidos station rates derived from model results. Mean annual rates for the 1998–2009 period are $P=5.65$ mm/day, $ET=2.72$ mm/day, and $Q=3.09$ mm/day. As discussed in section 3.1, simulated discharge is similar to the observations at Óbidos station, with a small bias equal to -4.6% . Mean precipitation, which is based on TRMM 3B42 v6 data, is slightly smaller ($\sim 6\%$) than values obtained in others: 6.0 mm/day from Espinoza *et al.* [2009] based on 756 pluviometric stations; 6.3 mm/day from Azarderakhsh *et al.* [2011] based on the Global Precipitation Climatology Project (GPCP) gauged and remote sensing data; 5.8 (5.2–8.6) mm/day by Marengo [2005] based on several rain gauges, remote sensing, and reanalyses-based data. ET rates are also comparable with values obtained in other studies, although there are large differences between them: 2.27 mm/day by Azarderakhsh *et al.* [2011] using global remote sensing-based products; 4.3 mm/day by Marengo [2005]; 3.23 mm/day by Ruhoff [2011] using MOD16 remote sensing product but including the Tocantins basin; and 3.2 mm/day (at Negro basin), 2.9–3.8 mm/day, and 2.6–3.0 mm/day using modeling results by Getirana *et al.* [2010], Costa and Foley [1997], and Beighley *et al.* [2009], respectively.

[46] Precipitation (P) exhibits a large seasonal variation, with larger rates ($P>7$ mm/day) between December and April with the maximum at February and March ($P \sim 8.5$ mm/day) and minimum values at July and August ($P \sim 2.5$ mm/day). The mean Amazon ET is almost constant along the year, without significant seasonal variations. The combination of P and ET rates causes a marked seasonal behavior in discharge, with maximum (minimum) values of 4.3

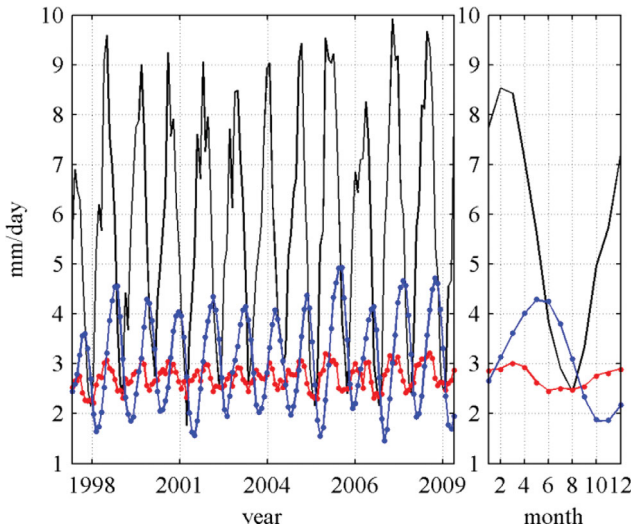


Figure 12. Water balance of the Amazon River basin. Monthly (left) and climatological (right) values of mean precipitation (black), evapotranspiration (red), and discharge close to the outlet at Óbidos (blue). Continuous lines (points) show simulation results (not) considering the influence of flood extent variability on evapotranspiration.

(1.9) mm/day, occurring in May–June (October–November). Discharge signal is delayed in 3 months if compared with P , showing the large water travel times along the Amazon rivers and floodplains.

[47] Although the seasonally inundated floodplains play an important role in water transport throughout the Amazonian rivers, as demonstrated by the sensitivity analysis and by the results shown in the next section, it seems not to have a major influence in water balance. Figure 12 shows a comparison of Q and ET results from two simulations, one considering the effect of seasonal flooded areas on ET [using methods described in Paiva et al., 2011a] and the other without such consideration, and the differences between them are insignificant. Although this is a preliminary analysis and as ET from flooded forests is not completely represented using the Penman Monteith approach, a possible explanation could be that (1) flooded areas represent a small part (less than 5%) of the total area of the Amazon and that (2) ET in the Amazon is driven mostly by radiation [Costa et al., 2010] and not by water availability and consequently ET rates from flooded and nonflooded forests are similar.

5.2. Terrestrial Water Storage

[48] In this section, the Amazon TWS changes and the role of surface, soil, and ground waters on TWS are explored. Analyses of Figure 9 based on GRACE data show a marked seasonal variability of TWS with large amplitude of variation (325 mm, mean of all GRACE solutions). Larger TWS variations are found mostly in central Amazon, with amplitudes of TWS larger than 750 mm, and smaller values are found in the Andean region (<300 mm). To evaluate the main contributors of the TWS variations, we computed the water storage of three major hydrological compartments using model results, namely surface water

(sum of river, floodplain, and surface runoff storages), soil water, and ground water, and calculated the respective amplitude of variation as described in section 2. The amplitude of variation of surface waters governs most of TWS changes in the Amazon basin (see Figure 13), mostly in central Amazon and areas with large floodplains (see Figures 7 and 13a). Soil water presents an important contribution on TWS changes in south-eastern areas, whereas ground water is the least important compartment in almost all regions. Surface waters dominate TWS variations for the whole Amazon area with a fraction of 56%, followed by soil (27%) and ground water storages (8%; see Figure 13b). In addition, surface and soil water present similar seasonal variation, whereas groundwater storage presents a small delay. Results agree with Han et al. [2009] and Frappart et al. [2008], which indicated the dominant role of surface waters in TWS variations in the Amazon. The results also agree with Frappart et al. [2011a] that, using mostly remotely sensed data sets at the Negro river basin, showed that TWS changes are dominated by surface waters followed by soil and ground water with similar importance. Our results are also similar with Kim et al.’s [2009] estimates for the Amazon in a global study using modeling results, where river storage including shallow ground water (soil moisture) explained 73% (27%) of total TWS changes.

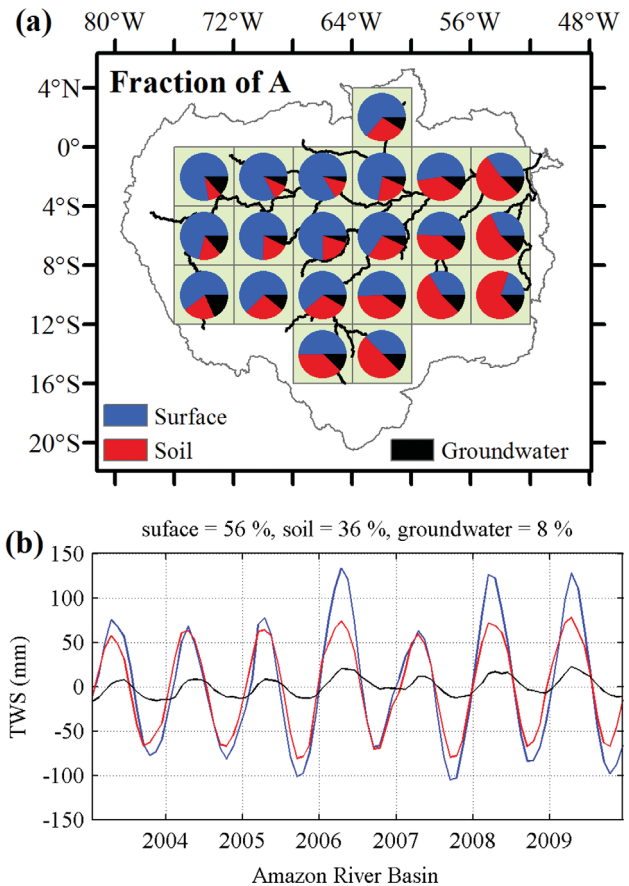


Figure 13. Fraction of terrestrial water storage divided into surface, soil, and ground waters. (a) Spatial distribution of the fraction of TWS amplitude from each hydrological compartment. (b) Monthly time series of TWS from surface (blue), soil (red), and ground (black) waters.

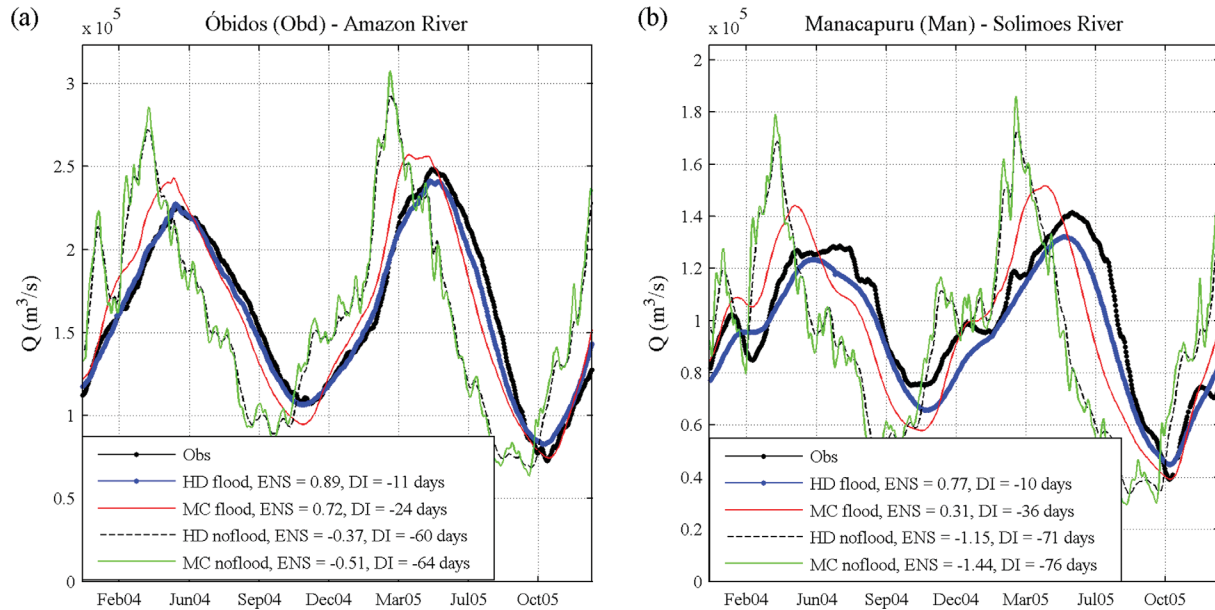


Figure 14. Observed (black line with dots) and simulated discharges at Óbidos (a) and Manacapuru (b) sites using hydrodynamic model with floodplains (blue line with dots), Muskingum Cunge with floodplains (red line), hydrodynamic model without floodplains (dashed black line), and Muskingum Cunge model without floodplains (gray line).

5.3. River-Floodplain Hydraulics

[49] To finish our analyses of the Amazon hydrological processes, river and floodplain processes are investigated, and the importance of backwater effects and flood inundation in stream flow routing is evaluated. We compared discharge results from four model runs using the same parameters and model input forcings in all of them, but with different kinds of stream flow routing methods: (1) HDf, HD model with floodplains, equal to model configuration used in the rest of the manuscript; (2) MCf, MC with floodplains, using a nonlinear version of the MC as presented by *Todini* [2007] and extended by *Pontes* [2011] to consider floodplains; (3) HDn, HD model without floodplains; and (4) MCn, MC without floodplains. The MC-based models, MCf and MCn, do not deal with backwater effects, as they are based on a kinematic wave approximation of the *Saint Venant* equations and do not consider neither the inertia nor the pressure forces, whereas HDn and MCn models do not represent flood inundation.

[50] Results shown in Figure 14 and in Table 2 indicate the better performance of the complete HD model (HDf) in comparison with the other methods. Including backwater effects and floodplain storage generally delay and attenuates hydrographs, and simulations agree with observations (e.g., $E_{NS}=0.89$ and 0.77 and $DI=-11$ and -10 days at Óbidos and Manacapuru stations, respectively). Neither considering backwater effects nor floodplains (MC run) causes very advanced ($DI=-64$ and -76 days) and noisy hydrographs, with low E_{NS} values ($E_{NS}=-0.51$ and -1.44) and discarding only flood inundation (HDn run) cause a similar effect. However, to include floodplains only (MCf) is not sufficient to reproduce observed discharges ($E_{NS}=0.72$ and 0.31), and hydrographs still advanced about 15 and 25 days if compared with the most complete model (HDf). Possibly, the influence of floodplains is increased when the pressure term is present, as discussed in *Paiva et al.* [2012].

[51] These results suggest that floodplains play a major role in flood wave attenuation and delay; however,

Table 2. Discharge Model Performance Statistics of Nash and Sutcliffe Index (E_{NS}) and Delay Index (DI, days) at Gauging Stations Presented in Figure 1^a

Gauge	River	E_{NS}				DI (days)			
		HDf	MCf	HDn	MCn	HDf	MCf	HDn	MCn
Jap	Japurá	0.21	0.22	0.11	0.1	-21	-21	-27	-27
Mou	Negro	0.65	0.66	0.49	0.45	5	-6	-24	-26
Pur	Purus	0.91	0.74	0.66	0.61	-6	-18	-22	-24
Faz	Madeira	0.92	0.88	0.63	0.54	8	-4	-26	-29
Ita	Tapajós	0.87	0.84	0.85	0.85	-2	9	-5	-5
Tam	Solimões	0.74	0.67	0.21	0.04	-3	-11	-35	-39
Man	Solimões	0.77	0.31	-1.15	-1.44	-10	-36	-71	-76
Obd	Amazon	0.89	0.72	-0.37	-0.51	-11	-24	-60	-64

^aThe simulations used were as follows: hydrodynamic model with and without floodplain (HDf and HDn, respectively) and Muskingum Cunge model with and without floodplain (MCf and MCn, respectively).

backwater effects also cause important impacts. The results are in accordance with preliminary analyses from Paiva et al. [2012]; however, they disagree with Yamazaki et al. [2011], who presented similar conclusions about floodplain storage but stated that backwater effects have a minor impact on hydrographs and are more important for representing water level profiles.

[52] Although discussions from previous sections indicate that the model errors may arise from uncertainty in input data, results from this section show the importance of the model structure. Our approach is relatively complex in terms of river hydraulics as it uses full *Saint Venant* equations, but is somehow simplified in terms of floodplain simulation. Consequently, it cannot fully represent all aspects of floodplain hydrodynamics such as bidirectional flows and river-floodplain water level dynamics [Alsdorf et al., 2003, 2007; Bonnet et al., 2008] and flow in small floodplain channels [Trigg et al., 2012]. We believe that different flood inundation approaches [e.g., Bonnet et al., 2008; Paz et al., 2011; Wilson et al., 2007; Bates and De Roo, 2000; Neal et al., 2012] coupled with full HD models should still be tested to check its feasibility to represent all floodplain processes and the influence of these processes in large-scale stream flow routing and inundation dynamics.

6. Summary and Conclusions

[53] We present an extensive validation of the physically based large-scale hydrologic and HD model MGB-IPH in the Amazon River basin using in situ and remote sensing datasets. Sources of model errors, which can be extrapolated to other similar large-scale models, were investigated by using model validation results and also supported by sensitivity tests. Finally, aspects of the physical functioning of the Amazon River basin are discussed taking advantage of the model results.

[54] The model is able to reproduce observed hydrographs at different spatial scales, although performance is usually better in large rivers with large flood wave travel times. The model provides feasible water level results in most of the gauging stations and also at altimetry-based validation sites and overall inundation extent results similar to the remote sensing estimates. Discharge is well simulated even in regions where other hydrological variables are not well represented, as in the lower Amazon where some errors in water levels and flood extent can be found. TWS results also agree with GRACE-derived estimates.

[55] Results from the sensitivity analysis indicate that model input data uncertainty may play an important role in model errors such as the ones presented in the model validation, although part of them can be due to the uncertainty in remote sensing data used here as observations. Precipitation forcing is the most sensitive variable, causing significant errors in mean discharge, water depth, and flood extent. At the same time, important errors occur in westerly areas, which may be a consequence of the poor quality of TRMM 3B42 rainfall data sets in these areas, which are mountainous and/or poorly monitored.

[56] The model results are also very sensitive to river-floodplain parameters, including river width and bottom level, Manning's roughness coefficient, and floodplain bathymetry. Important interactions between water levels,

flooded areas, and discharge errors are observed during the floodwaves traveling. Uncertainty in river and floodplain geometry, estimated through geomorphological relations and the SRTM DEM, causes errors in simulated water levels and inundation extent in some areas, indicating the need for improving current parameter estimation methods. These parameters are similar to the ones required in other large-scale models, and its uncertainty may cause errors in these models as well. Some alternatives to that could be the usage of newly remote sensing techniques for parameter estimation or corrections of the SRTM DEM to remove vegetation height in forested areas and to estimate bottom level of floodplains.

[57] Overall water balance derived from model results is similar to estimates from previous studies. Mean annual rates of precipitation, evapotranspiration, and discharge at Óbidos station are $P=5.65$ mm/day, $ET=2.72$ mm/day, and $Q=3.09$ mm/day, respectively. TWS changes show marked seasonal variability with a large amplitude of variation of 325 mm for all Amazon, and larger amplitude values (>750 mm) are found in central Amazon. Surface waters govern most of TWS changes in the Amazon basin (56%), mostly in central Amazon and in areas with large floodplains, whereas soil water presents an important contribution to TWS changes (27%), mainly in south-eastern areas and groundwater, it is the less important hydrological compartment (8%).

[58] Finally, river and floodplain processes and the importance of backwater effects and flood inundation in stream flow routing were investigated. Results suggest that floodplains play a major role in flood wave attenuation and delay; however, backwater effects also cause important impacts, indicating the importance of including a flood inundation module and a complex *Saint Venant* equation approximation for river floodplain processes modeling in the Amazon. In contrast, although the seasonally inundated floodplains play an important role in water transport along Amazonian rivers, it seems not to have a major influence on evapotranspiration and water balance.

[59] **Acknowledgments.** The authors are grateful for the financial and operational support from the Brazilian agencies FINEP and ANA (Projeto de Integração e Cooperação Amazônica para a Modernização do Monitoramento Hidrológico (ICA-MMH)) and CNPq (Assimilação de Dados de monitoramento Espacial para a análise do regime hidrológico da Bacia Amazônica e a previsão de curto e médio prazos) and the MHYZPA project funded by the French INSU EC2CO Cytrix program; the global inundation extent data set provided by Fabrice Papa; the ENVISAT satellite altimetry data provided by Joecila Santos da Silva; the TRMM data supplied by NASA and associated agencies; the discharge data provided by ANA, HYBAM, SENHAMI-Peru, and SENHAMI-Bolivia; and for the constructive comments from Praveen Kumar, Editor of *Water Resources Research*, Augusto Getirana, and other two anonymous reviewers.

References

- Alsdorf, D., T. Dunne, J. Melack, L. Smith, and L. Hess (2003), Diffusion modeling of recession flow on central Amazonian floodplains, *Geophys. Res. Lett.*, *32*(21), L21405, doi:10.1029/2005GL024412.
- Alsdorf, D., P. Bates, J. Melack, M. Wilson, and T. Dunne (2007a), The spatial and temporal complexity of the Amazon flood measured from space, *Geophys. Res. Lett.*, *34*(8), L08402, doi:10.1029/2007GL029447.
- Alsdorf, D. E., E. Rodriguez, and D. P. Lettenmaier (2007b), Measuring surface water from space, *Rev. Geophys.*, *45*, RG2002, doi:10.1029/2006RG000197.
- Alsdorf, D., S.-C. Han, P. Bates, and J. Melack (2010), Seasonal water storage on the Amazon floodplain measured from satellites, *Remote Sens. Environ.*, *114*, 2448–2456.

- Azarderakhsh, M., W. B. Rossow, F. Papa, H. Norouzi, and R. Khanbilvardi (2011), Diagnosing water variations within the Amazon basin using satellite data, *J. Geophys. Res.*, *116*, D24107, doi:10.1029/2011JD015997.
- Bates, P. D., and A. P. J. De Roo (2000), A simple raster based model for flood inundation simulation, *J. Hydrol.*, *236*, 54–77.
- Beighley, R. E., K. G. Eggert, T. Dunne, Y. He, V. Gummadi, and K. L. Verdin (2009), Simulating hydrologic and hydraulic processes throughout the Amazon River Basin, *Hydrol. Processes*, *23*(8), 1221–1235.
- Biancamaria, S., P. D. Bates, A. Boone, and N. M. Mognard (2009), Large-scale coupled hydrologic and hydraulic modelling of the Ob river in Siberia, *J. Hydrol.*, *379*, 136–150.
- Bonnet, M. P., et al. (2008), Floodplain hydrology in an Amazon floodplain lake (Lago Grande de Curuai), *J. Hydrol.*, *349*, 18–30.
- Bourgoin, L. M., M. P. Bonnet, J. M. Martinez, P. Kosuth, G. Cochonneau, P. M. Turcq, J. L. Guyot, P. Vauchel, N. Filizola, and P. Seyler (2007), Temporal dynamics of water and sediment exchanges between the Curuai floodplain and the Amazon River, Brazil, *J. Hydrol.*, *335*, 140–156.
- Castellarin, A., G. Di Baldassarre, P. D. Bates, and A. Brath (2009), Optimal cross-sectional spacing in Preissmann scheme 1D hydrodynamic models, *J. Hydraul. Eng.*, *135*(2), 96–105.
- Chen, J. L., C. R. Wilson, and B. D. Tapley (2010), The 2009 exceptional Amazon flood and interannual terrestrial water storage change observed by GRACE, *Water Resour. Res.*, *46*, W12526, doi:10.1029/2010WR009383.
- Coe, M. T., M. H. Costa, and E. A. Howard (2008), Simulating the surface waters of the Amazon River basin: Impacts of new river geomorphic and flow parameterizations, *Hydrol. Processes*, *22*(14), 2542–2553.
- Collischonn, W. (2001), Hydrologic simulation of large basins [in Portuguese], Ph.D. thesis, Inst. de Pesqui. Hidraul., Univ. Fed. do Rio Grande do Sul, Porto Alegre, Brazil.
- Collischonn, W., D. G. Allasia, B. C. Silva, and C. E. M. Tucci (2007), The MGB-IPH model for large-scale rainfall-runoff modeling, *Hydrol. Sci. J.*, *52*, 878–895.
- Collischonn, B., W. Collischonn, and C. Tucci (2008), Daily hydrological modeling in the Amazon basin using TRMM rainfall estimates, *J. Hydrol.*, *360*, 207–216.
- Condom, T., P. Rau, and J. C. Espinoza (2010), Correction of TRMM 3B43 monthly precipitation data over the mountainous areas of Peru during the period 1998–2007, *Hydrol. Processes*, *25*, 1924–1933, doi:10.1002/hyp.7949.
- Costa, M. H., and J. A. Foley (1997), Water balance of the Amazon Basin: Dependence on vegetation cover and canopy conductance, *J. Geophys. Res.*, *102*(D20), 23973–23989.
- Costa, M. H., M. C. Biajoli, L. Sanches, A. C. M. Malhado, L. R. Hutyra, H. R. da Rocha, R. G. Aguiar, and A. C. de Araújo (2010), Atmospheric versus vegetation controls of Amazonian tropical rain forest evapotranspiration: Are the wet and seasonally dry rain forests any different?, *J. Geophys. Res.*, *115*, G04021, doi:10.1029/2009JG001179.
- Cunge, J. A., F. M. Holly, and A. Verney (1980), *Practical Aspects of Computational River Hydraulics*, Pitman Advanced Publishing Program, London.
- Decharme, B., R. Alkama, F. Papa, S. Faroux, H. Douville, and C. Prigent (2011), Global off-line evaluation of the ISBA-TRIP flood model, *Clim. Dyn.*, *38*, 1389–1412.
- Dijkshoorn, J. A., J. R. M. Hutting, and P. Tempel (2005), Update of the 1:5 million soil and terrain database for Latin America and the Caribbean (SOTERLAC; version 2.0), *Rep. 2005/01*, ISRIC-World Soil Information, Wageningen, Netherlands.
- Durand, M., E. Rodríguez, D. Alsdorf, and M. Trigg (2010a), Estimating river depth from remote sensing swath interferometry measurements of river, *IEEE J. Sel. Top. Appl. Earth Obs. Remote Sens.*, *3*, 20–31.
- Durand, M., L. L. Fu, D. P. Lettenmaier, D. E. Alsdorf, E. Rodríguez, and D. E. Fernandez (2010b), The surface water and ocean topography mission: Observing terrestrial surface water and oceanic submesoscale eddies, *Proc. IEEE*, *98*(5), 766–779.
- Espinoza, J. C., J. Ronchail, J. L. Guyot, G. Cocheneau, N. Filizola, W. Lavado, E. de Oliveira, R. Pombosa, and P. Vauchel (2009), Spatio-temporal rainfall variability in the Amazon Basin countries (Brazil, Peru, Bolivia, Colombia and Ecuador), *Int. J. Climatol.*, *29*, 1574–1594.
- Espinoza, J. C., J. Ronchail, J. L. Guyot, C. Junquas, P. Vauchel, W. Lavado, G. Drapeau, and R. Pombosa (2011), Climate variability and extreme drought in the upper Solimões River (western Amazon Basin): Understanding the exceptional 2010 drought, *Geophys. Res. Lett.*, *38*, L13406, doi:10.1029/2011GL047862.
- Eva, H. D., E. E. De Miranda, C. M. Di Bella, and V. Gond (2002), A vegetation map of South America, EUR 20159 EN, European Commission, Luxembourg.
- Farr, T. G., et al. (2007), The shuttle radar topography mission, *Rev. Geophys.*, *45*, RG2004, doi:10.1029/2005RG000183.
- Frappart, F., F. Papa, J. S. Famiglietti, C. Prigent, W. B. Rossow, and F. Seyler (2008), Interannual variations of river water storage from a multiple satellite approach: A case study for the Rio Negro River basin, *J. Geophys. Res.*, *113*, D21104, doi:10.1029/2007JD009438.
- Frappart, F., G. Ramillien, P. Maisongrande, and M.-P. Bonnet (2010), Denoising satellite gravity signals by independent component analysis, *IEEE Geosci. Remote Sens. Lett.*, *7*(3), 421–425, doi:10.1109/LGRS.2009.2037837.
- Frappart, F., et al. (2011a), Satellite-based estimates of groundwater storage variations in large drainage basins with extensive floodplains, *Remote Sens. Environ.*, *115*(6), 1588–1594.
- Frappart, F., G. Ramillien, M. Leblanc, S. O. Tweed, M.-P. Bonnet, and P. Maisongrande (2011b), An independent component analysis approach for filtering continental hydrology in the GRACE gravity data, *Remote Sens. Environ.*, *115*(1), 187–204, doi:10.1016/j.rse.2010.08.017.
- Getirana, A. C. V., M.-P. Bonnet, O. C. Rotunno Filho, W. Collischonn, J.-L. Guyot, F. Seyler, and W. J. Mansur (2010), Hydrological modeling and water balance of the Negro River basin: Evaluation based on in situ and spatial altimetry data, *Hydrol. Processes*, *24*(22), 3219–3236.
- Getirana, A. C. V., et al. (2011), Calibração e Validação de Modelo Hidrológico com Observações In Situ, Altimetria e Gravimetria Espaciais, *Rev. Bras. Recursos Hídricos*, *16*(1), 29–45.
- Getirana, A. C. V., A. Boone, D. Yamazaki, B. Decharme, F. Papa, and N. Mognard (2012), The hydrological modeling and analysis platform (HyMAP): Evaluation in the Amazon basin, *J. Hydrometeorol.*, *13*, 1641–1665.
- Han, S.-C., H. Kim, I.-Y. Yeo, P. Yeh, T. Oki, K.-W. Seo, D. Alsdorf, and S. B. Luthcke (2009), Dynamics of surface water storage in the Amazon inferred from measurements of inter-satellite distance change, *Geophys. Res. Lett.*, *36*, L09403, doi:10.1029/2009GL037910.
- Hess, L. L., J. M. Melack, E. M. L. M. Novo, C. C. F. Barbosa, and M. Gastil (2003), Dual-season mapping of wetland inundation and vegetation for the central Amazon basin, *Remote Sens. Environ.*, *87*, 404–428.
- Huffman, G., R. Adler, D. Bolvin, G. Gu, E. Nelkin, K. Bowman, Y. Hong, E. Stocker, and D. Wolff (2007), The TRMM multisatellite precipitation analysis (TCMA): Quasi-global, multiyear, combined-sensor precipitation estimates at fine scales, *J. Hydrometeorol.*, *8*, 38–55.
- Junk, W. J. (1997), General aspects of floodplain ecology with special reference to Amazonian floodplains, in *The Central-Amazonian Floodplain: Ecology of a Pulsing System, Ecological Studies*, edited by W. J. Junk, pp. 3–22, Springer, Heidelberg.
- Kim, H., P. J.-F. Yeh, T. Oki, and S. Kanae (2009), Role of rivers in the seasonal variations of terrestrial water storage over global basins, *Geophys. Res. Lett.*, *36*, L17402, doi:10.1029/2009GL039006.
- Kosuth, P., J. Callède, A. Laraque, N. Filizola, J. L. Guyot, P. Seyler, J. M. Fritsch, and V. Guimaraes (2009), Sea-tide effects on flows in the lower reaches of the Amazon River, *Hydrol. Processes*, *23*(22), 3141–3150.
- Lian, Y., I.-C. Chan, J. Singh, M. Demissie, V. Knapp, and H. Xie (2007), Coupling of hydrologic and hydraulic models for the Illinois River Basin, *J. Hydrol.*, *344*, 210–222.
- Marengo, J. A. (2005), Characteristics and spatio-temporal variability of the Amazon River basin water budget, *Clim. Dyn.*, *24*, 11–22, doi:10.1007/s00382-004-0461-6.
- Marengo, J., C. Nobre, J. Tomasella, M. Oyama, G. de Oliveira, R. de Oliveira, H. Camargo, and L. Alves (2008), The drought in Amazonia in 2005, *J. Clim.*, *21*, 495–516.
- Marengo, J. A., J. Tomasella, L. M. Alves, W. R. Soares, and D. A. Rodriguez (2011), The drought of 2010 in the context of historical droughts in the Amazon region, *Geophys. Res. Lett.*, *38*, L12703, doi:10.1029/2011GL047436.
- Meade, R. H., J. M. Rayol, S. C. Da Conceição, and J. R. G. Natividade (1991), Backwater effects in the Amazon River basin of Brazil, *Environ. Geol. Water Sci.*, *18*(2), 105–114.
- Melack, J. M., and L. L. Hess (2010), Remote sensing of the distribution and extent of wetlands in the Amazon basin, in *Amazonian Floodplain Forests: Ecophysiology, Ecology, Biodiversity and Sustainable Management, Ecological Studies*, Part 1, vol. 210, edited by W. J. Junk et al., pp. 43–59, Springer, Dordrecht.
- Melack, J. M., L. L. Hess, M. Gastil, B. R. Forsberg, S. K. Hamilton, I. B. T. Lima, and E. M. L. M. Novo (2004), Regionalization of methane emissions in the Amazon basin with microwave remote sensing, *Global Change Biol.*, *10*, 530–544.

- Mohamed, Y. A., B. J. J. M. van den Hurk, H. H. G. Savenije, and W. G. M. Bastiaanssen (2005), Impact of the Sudd wetland on the Nile hydroclimatology, *Water Resour. Res.*, *41*, W08420, doi:10.1029/2004WR003792.
- New, M., D. Lister, M. Hulme, and I. Makin (2002), A high-resolution data set of surface climate over global land areas, *Clim. Res.*, *21*, 1–25.
- Neal, J. C., G. J.-P. Schumann, and P. D. D. Bates (2012), A sub-grid channel model for simulating river hydraulics and floodplain inundation over large and data sparse areas, *Water Resour. Res.*, *48*, W11506, doi:10.1029/2012WR012514.
- Paiva, R. C. D., W. Collischonn, and C. E. M. Tucci (2011a), Large scale hydrologic and hydrodynamic modeling using limited data and a GIS based approach, *J. Hydrol.*, *406*, 170–181.
- Paiva, R. C. D., D. C. Buarque, R. T. Clarke, W. Collischonn, and D. G. Allasia (2011b), Reduced precipitation over large water bodies in the Brazilian Amazon shown from TRMM data, *Geophys. Res. Lett.*, *38*, L04406, doi:10.1029/2010GL045277.
- Paiva, R. C. D., W. Collischonn, and D. C. Buarque (2012), Validation of a full hydrodynamic model for large scale hydrologic modelling in the Amazon, *Hydrol. Processes*, doi:10.1002/hyp.8425.
- Papa, F., C. Prigent, F. Aires, C. Jimenez, W. B. Rossow, and E. Matthews (2010), Interannual variability of surface water extent at the global scale, 1993–2004, *J. Geophys. Res.*, *115*, D12111, doi:10.1029/2009JD012674.
- Paz, A. R., J. M. Bravo, D. Allasia, W. Collischonn, and C. E. M. Tucci (2010), Large-scale hydrodynamic modeling of a complex river network and floodplains, *J. Hydrol. Eng.*, *15*(2), 152–165.
- Paz, A. R. D., W. Collischonn, C. E. M. Tucci, and C. R. Padovani (2011), Large-scale modelling of channel flow and floodplain inundation dynamics and its application to the Pantanal (Brazil), *Hydrol. Processes*, *25*, 1498–1516, doi:10.1002/hyp.7926.
- Ponce, V. M. (1989), *Engineering Hydrology*, Prentice Hall, Englewood Cliffs, N. J.
- Pontes, P. R. M. (2011), Comparing simplified hydrodynamic models for flow routing in rivers and channels [in Portuguese], Ph.D. thesis, Inst. de Pesqui. Hidraul., Univ. Fed. do Rio Grande do Sul, Porto Alegre, Brazil. [Available at <http://hdl.handle.net/10183/35350>.]
- Prigent, C., F. Papa, F. Aires, W. B. Rossow, and E. Matthews (2007), Global inundation dynamics inferred from multiple satellite observations, 1993–2000, *J. Geophys. Res.*, *112*, D12107, doi:10.1029/2006JD007847.
- Prigent, C., N. Rochetin, F. Aires, E. Defer, J.-Y. Grandpeix, C. Jimenez, and F. Papa (2011), Impact of the inundation occurrence on the deep convection at continental scale from satellite observations and modeling experiments, *J. Geophys. Res.*, *116*, D24118, doi:10.1029/2011JD016311.
- RADAMBRASIL (1982), Programa de Integração Nacional, Levantamento de Recursos Naturais, Ministério das Minas e Energia, Secretaria-Geral.
- Ramillien, G., F. Frappart, A. Cazenave, and A. Güntner (2005), Time variations of the land water storage from an inversion of 2 years of GRACE geoids, *Earth Planet. Sci. Lett.*, *235*, 283–301, doi:10.1016/j.epsl.2005.04.005.
- Ramillien, G., J. S. Famiglietti, and J. Wahr (2008), Detection of continental hydrology and glaciology signals from GRACE: A review, *Surv. Geophys.*, *29*(4/5), 361–374, doi:10.1007/s10712-008-9048-9.
- Rennó, C. D., A. D. Nobre, L. A. Cuartas, J. V. Soares, M. G. Hodnett, J. Tomasella, and M. J. Waterloo (2008), HAND, a new terrain descriptor using SRTM-DEM: Mapping terra-firme rainforest environments in Amazonia, *Remote Sens. Environ.*, *12*(9), 3469–3481.
- Richey, J. E., J. M. Melack, A. K. Aufdenkampe, V. M. Ballester, and L. L. Hess (2002), Outgassing from Amazonian rivers and wetlands as a large tropical source of atmospheric CO₂, *Nature*, *416*, 617–620.
- Ruhoff, A. L. (2011), Remote sensing applied to evapotranspiration estimation in tropical biomes [in Portuguese], Ph.D. thesis, Inst. de Pesqui. Hidraul., Univ. Fed. do Rio Grande do Sul, Porto Alegre, Brazil. [Available at <http://hdl.handle.net/10183/32468>.]
- Santos da Silva, J., S. Calmant, F. Seyler, O. C. Rotunno Filho, G. Cochonneau, and W. J. Mansur (2010), Water levels in the Amazon basin derived from the ERS 2 and ENVISAT radar altimetry missions, *Remote Sens. Environ.*, *114*(10), 2160–2181.
- Schmidt, R., F. Flechtner, U. Meyer, K.-H. Neumayer, C. Dahle, R. Koenig, J. Kusche (2008), Hydrological signals observed by the GRACE satellites, *Surv. Geophys.*, *29*, 319–334, doi:10.1007/s10712-008-9033-3.
- Seyler, P., and G. R. Boaventura (2003), Distribution and partition of trace metals in the Amazon basin, *Hydrol. Processes*, *17*, 1345–1361.
- Simard, M., N. Pinto, J. Fisher, and A. Baccini (2011), Mapping forest canopy height globally with spaceborne lidar, *J. Geophys. Res.*, *116*, G04021, doi:10.1029/2011JG001708.
- Shuttleworth, W. J. (1993), Evaporation, in *Handbook of Hydrology*, edited by D. R. Maidment, McGraw-Hill, New York.
- Sun, G., K. J. Ranson, V. I. Kharuk, and K. Kovacs (2003), Validation of surface height from shuttle radar topography mission using shuttle laser altimeter, *Remote Sens. Environ.*, *88*, 401–411.
- Tapley, B. D., S. Bettadpur, J. C. Ries, P. F. Thompson, and M. Watkins (2004), GRACE measurements of mass variability in the Earth system, *Science*, *305*, 503–505.
- Tian, Y., and C. D. Peters-Lidard (2010), A global map of uncertainties in satellite-based precipitation measurements, *Geophys. Res. Lett.*, *37*, L24407, doi:10.1029/2010GL046008.
- Todini, E. (2007), A mass conservative and water storage consistent variable parameter Muskingum-Cunge approach, *Hydrol. Earth Syst. Sci.*, *11*, 1645–1659, doi:10.5194/hess-11-1645-2007.
- Tomasella, J., L. S. Borma, J. A. Marengo, D. A. Rodriguez, L. A. Cuartas, C. A. Nobre, and M. C. R. Prado (2010), The droughts of 1996–1997 and 2004–2005 in Amazonia: Hydrological response in the river main-stem, *Hydrol. Processes*, *25*, 1228–1242.
- Trigg, M. A., M. D. Wilson, P. D. Bates, M. S. Horritt, D. E. Alsdorf, B. R. Forsberg, and M. C. Vega (2009), Amazon flood wave hydraulics, *J. Hydrol.*, *374*, 92–105.
- Trigg, M. A., P. D. D. Bates, M. D. Wilson, G. J.-P. Schumann, and C. A. Baugh (2012), Floodplain channel morphology and networks of the middle Amazon River, *Water Resour. Res.*, *48*, W10504, doi:10.1029/2012WR011888.
- Wilson, W., P. Bates, D. Alsdorf, B. Forsberg, M. Horritt, J. Melack, F. Frappart, and J. Famiglietti (2007), Modeling large-scale inundation of Amazonian seasonally flooded wetlands, *Geophys. Res. Lett.*, *34*, L15404, doi:10.1029/2007GL030156.
- Yapo, P. O., H. V. Gupta, and S. Sorooshian (1998), Multi-objective global optimization for hydrologic models, *J. Hydrol.*, *204*, 83–97.
- Yamazaki, D., S. Kanae, H. Kim, and T. Oki (2011), A physically based description of floodplain inundation dynamics in a global river routing model, *Water Resour. Res.*, *47*, W04501, doi:10.1029/2010WR009726.
- Yamazaki, D., C. Baugh, P. D. Bates, S. Kanae, D. E. Alsdorf, and T. Oki (2012a), Adjustment of a spaceborne DEM for use in floodplain hydrodynamic modelling, *J. Hydrol.*, *436/437*, 81–91, doi:10.1016/j.jhydrol.2012.02.045.
- Yamazaki, D., H. Lee, D. E. Alsdorf, E. Dutra, H. Kim, S. Kanae, and T. Oki (2012b), Analysis of the water level dynamics simulated by a global river model: A case study in the Amazon River, *Water Resour. Res.*, *48*, W09508, doi:10.1029/2012WR011869.